Journal of Structural Geology 180 (2024) 105088

Contents lists available at ScienceDirect

Journal of Structural Geology

journal homepage: www.elsevier.com/locate/jsg

Overprinting orogenic events, ductile extrusion and strain partitioning during Caledonian transpression, NW Mainland Shetland

Timothy B. Armitage [a,b], Robert E. Holdsworth [a,*], Robin A. Strachan [c], Edward D. Dempsey [d], Richard J. Walker [e], Diana T. Alvarez-Ruiz [f], Geoffrey E. Lloyd [g]

[a] Department of Earth Sciences, Durham University, Durham, DH1 3LE, UK
[b] British Geological Survey, The Lyell Centre, Research Avenue South, Edinburgh EH14 4AP, UK
[c] School of the Environment, Geography and Geoscience, University of Portsmouth, Portsmouth, PO1 3QL, UK
[d] Department of Geography, Geology and Environment, University of Hull, Hull, HU6 7RX, UK
[e] University of California, Davis, USA
[f] Department of Physics, G.J. Russell Microscopy Facility, Durham University, Durham, UK
[g] Institute of Geophysics and Tectonics, School of Earth and Environment, University of Leeds, Leeds, LS2 9JT, UK

ARTICLE INFO

Keywords:
Transpression
Strain partitioning
Overprinting events
Quartz petrofabric analysis
EBSD

ABSTRACT

A 3.6 km thick stack of mid-crustal deformed Precambrian rocks is associated with the North Roe Nappe (NRN) and Walls Boundary Fault in the northernmost Scottish Caledonides on NW Mainland Shetland. The greenschist- to amphibolite-facies rocks display unusually complex and heterogeneous combinations of coaxial and non-coaxial transpressional deformation. Previously published isotopic dating, together with new detailed field mapping and microstructural characterisation show that the NRN preserves a record of Neoarchaean, Neoproterozoic (Knoydartian) and Ordovician-Silurian (Caledonian) overprinting deformation and metamorphism. Neoarchaean events in the Uyea Gneiss Complex located in its footwall are reworked by younger events in the overlying nappe pile. The main ductile fabrics were formed during Caledonian top-to-the W/NW thrusting and top-to-the N sinistral shearing, with subordinate regions of top- to-the E extensional and NNE-SSW dextral shearing. In lower parts of the NRN, these different kinematic domains are texturally indistinguishable and overprinting relationships are absent. At higher levels, top-to-the-W/NW thrust-related fabrics are consistently overprinted by top-to-the-N/NE sinistral shearing. The highly partitioned transpressional deformation shows similarities with equivalent rocks of the Moine Nappe in NW Scotland.

1. Introduction

The motions of irregular tectonic plates on a spherical planet mean that almost 60% of deformation zones related to present day - and by inference past - plate margins involve significant oblique convergence or divergence (e.g. Woodcock 1986). This leads to spatially and temporally varied combinations of three-dimensional, non-plane strain coaxial and non-coaxial deformation known as transpression and transtension zones (Harland 1971; Dewey et al., 1998). In the deeper parts of the crust (>10 km depth), such deformation zones commonly display anastomosing patterns of shear localization with local variations in thickness, kinematic patterns and finite strain that are challenging to analyse and understand (e.g. Jones et al., 2005).

Regional-scale shear zones are excellently preserved in the well-exposed Precambrian rocks of the northernmost Scottish Caledonides in Shetland (Fig. 1a–c). Shetland is located almost equidistant between mainland Scotland (part of Laurentia) and the western Scandinavian Caledonides in Norway (Baltica). Recent geochronological studies have clarified the timings of tectonic events in Shetland (e.g. Jahn et al., 2017; Walker et al., 2016, 2020; Cutts et al., 2009, 2011). However, no modern field and microstructural studies have been published detailing the structural evolution of the complexly deformed rocks in NW Shetland which lie between two key Caledonian regional structures: the supposed northward continuation of the Moine Thrust and the Walls Boundary Fault Zone (Fig. 1a and b). In this paper, we present a field mapping and microstructural study of the nature and kinematic patterns of ductile deformation found in these rocks, termed here the North Roe Nappe. This reveals a complex and highly partitioned pattern of deformation

* Corresponding author.
E-mail address: r.e.holdsworth@durham.ac.uk (R.E. Holdsworth).

https://doi.org/10.1016/j.jsg.2024.105088
Received 7 July 2023; Received in revised form 15 February 2024; Accepted 15 February 2024
Available online 21 February 2024

that can be related to a combination of overprinting orogenic events and oblique tectonic deformation processes.

1.1. Geological setting

1.1.1. Overview

The Caledonian orogeny in Scotland resulted from the closure of the Iapetus Ocean and is thought to comprise at least two distinct events: an early to middle Ordovician arc-continent collision (Grampian orogenic event), followed in the late Ordovician to Silurian by the culminating sinistrally oblique collision of Laurentia with combined Baltica and Avalonia (Scandian orogenic event) (Fig. 1c) (Soper et al., 1992; Strachan et al., 2020; Chew and Strachan 2014; Law et al., in press). The Scandian orogenic event was overlapped by regional-scale sinistral strike-slip faulting (Dewey and Strachan 2003). The Laurentian metasedimentary successions of the Northern Highland (NHT) and Grampian

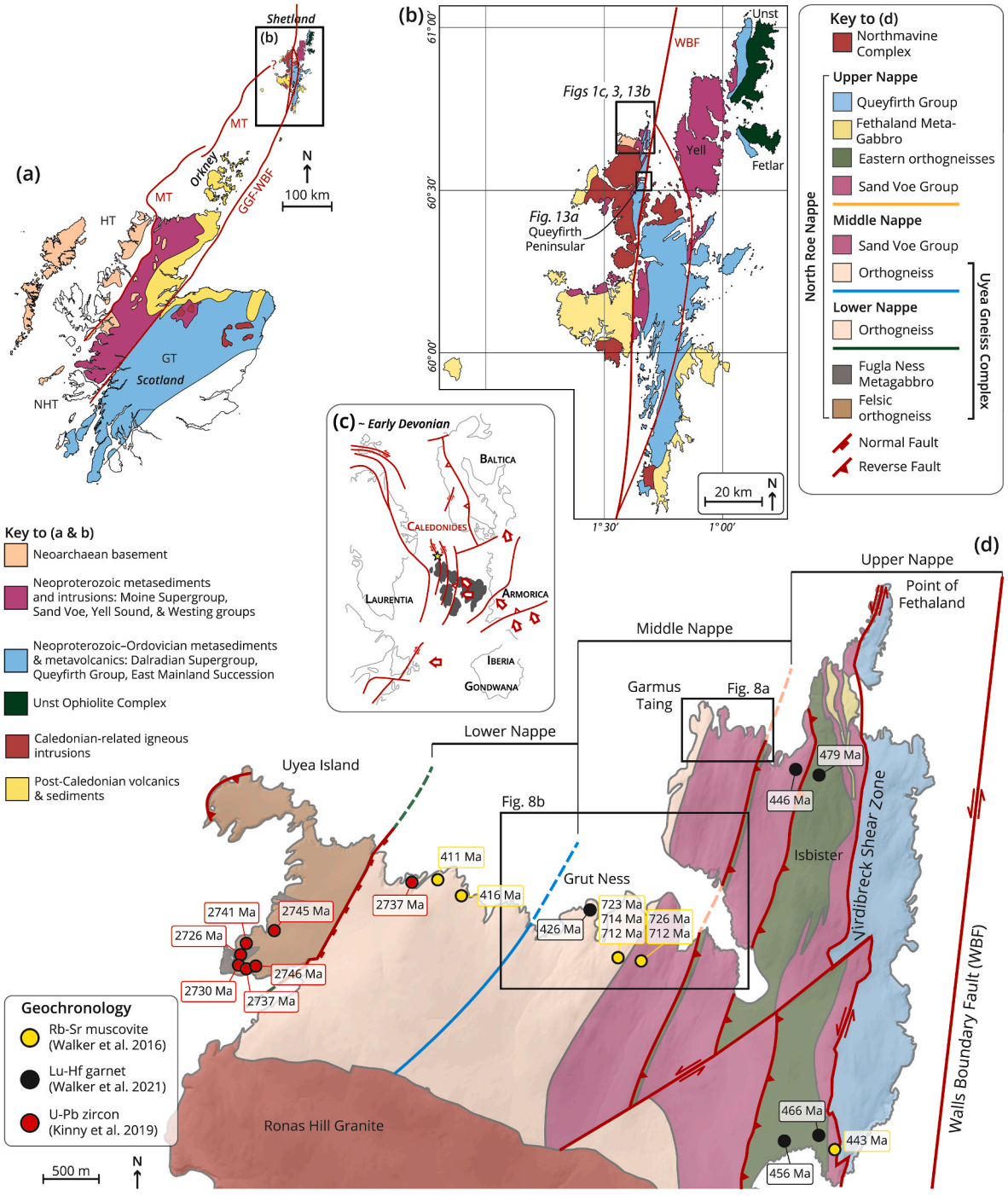

Fig. 1. Location of study area. **(a)** General sketch of NW Scotland, Orkney and Shetland showing the position of the Great Glen–Walls Boundary faults. **(b)** Regional map of Shetland showing the main tectonostratigraphic units and tract-bounding faults. GC, Graven Complex; GGF, Great Glen Fault; GT, Grampian Terrane; HT, Hebridean Terrane; MT, Moine Thrust; NHT, Northern Highland Terrane; WBF, Walls Boundary Fault. **(c)** An early Devonian palaeogeographic reconstruction of the N Atlantic region showing the location of Shetland relative to other regions. **(d)** Geological map of northwest Mainland Shetland, showing the major units, domains, domain bounding faults, brittle structures, locations for Fig. 8a and b. The ages and locations of previously dated samples, techniques used and source references are also shown.

(GT) terranes (Fig. 1a) and their lateral equivalents in Shetland underwent polyphase deformation and amphibolite to greenschist facies metamorphism. In Shetland, the most significant transcurrent fault is the N-S striking Walls Boundary Fault (WBF) (Fig. 1b and c; Flinn 1977, 1992; Watts et al., 2007; Armitage et al., 2021). This is widely viewed as being the northward continuation of the Great Glen Fault (GGF) of mainland Scotland (Fig. 1a; McGeary 1989; Flinn 1992). The WBF separates two regions of mainly metasedimentary rocks with Laurentian affinities that have been correlated with successions along strike in mainland Scotland (Fig. 1a and b).

East of the WBF, the early Neoproterozoic psammitic and pelitic gneisses of the Yell Sound and Westing groups have been correlated with the Moine Supergroup of mainland Scotland based on lithological similarity and similar detrital zircon populations (Flinn 1988; Jahn et al., 2017). They record evidence for amphibolite-facies metamorphism at c. 930–920 Ma (Cutts et al., 2009, 2011) and incorporate slivers of Archaean orthogneisses that likely represent the basement on which the Yell Sound and Westing groups were deposited (Jahn et al., 2017). Succeeding these units to the east, the psammites, marbles and metavolcanic rocks of the late Neoproterozoic–Cambrian East Mainland Succession may correlate with parts of the Dalradian Supergroup in Scotland (Fig. 1a and b; Flinn 1988; Prave et al., 2009; Strachan et al., 2013). Overlying the East Mainland Succession on Unst and Fetlar (Fig. 1b) is the Unst Ophiolite Complex which is thought to have been emplaced during the Grampian arc-continent collision (Spray 1988; Spray and Dunning 1991; Flinn 2014; Crowley and Strachan 2015).

West of the WBF in NW Mainland Shetland, the psammites of the Sand Voe Group (Fig. 1b) have been correlated on lithological grounds with parts of the Moine Supergroup (Flinn 1988). Immediately west of the WBF, the psammites, pelites, marbles and metamorphosed basic tuffs of the Queyfirth Group are thought to have Dalradian affinities (Mykura et al., 1976).

Integrated isotopic, structural and metamorphic studies indicate that the metasedimentary successions west and east of the WBF were affected by two main Caledonian orogenic events. Ophiolite obduction between c. 490 and 485 Ma was followed by Grampian regional deformation and amphibolite facies metamorphism between c. 485 and c. 465 Ma (Spray 1988; Cutts et al., 2011; Walker et al., 2016, 2020). East of the WBF, Grampian foliations are cross-cut by the undeformed Brae pluton which was emplaced at c. 465 Ma (Lancaster et al., 2017). Younger isotopic ages mainly fall between c. 450 and 430 Ma (Walker et al., 2016, 2020). It was thought that a series of c. 450-445 Lu-Hf and Sm-Nd garnet ages (also seen in the western Moine rocks of mainland NW Scotland) resulted from a second arc accretion event (Bird et al., 2013) or possibly flat-slab subduction (Dewey et al., 2015) before the final closure of Iapetus and Scandian collisional orogeny at c. 430 Ma. However, it now seems likely that outboard parts of the Baltican margin first collided with Laurentia at c. 450 Ma (Jakob et al., 2019, 2022) and hence the culminating Scandian orogeny may have occurred over the entire 450-430 Ma time span (Law et al., in press).

1.1.2. The North Roe Nappe

The northwesternmost part of Shetland is dominated by the North Roe Nappe (Fig. 1d and 2), composed of easterly-dipping meta-igneous and metasedimentary rocks. The basal shear zone of the nappe separates it from underlying Neoarchean basement of the Uyea Gneiss Complex (UGC; Fig. 1d). The UGC mainly comprises foliated granitic gneiss with subordinate metagabbro intrusions (Fugla Ness metagabbros; Kinny et al., 2019). Field evidence indicates that the metagabbro bodies were intruded soon after the host granitic gneiss had largely acquired its dominant foliation (Kinny et al., 2019). U-Pb zircon analyses obtained from both lithologies indicate igneous protolith ages of *c.* 2746–2726 Ma and subsequent metamorphism at c. 2710 Ma (Fig. 1d; Kinny et al., 2019). These allow correlation with the Lewisian Gneiss Complex that forms the basement of the Caledonian foreland in mainland Scotland (Fig. 1a; Holdsworth et al., 2019). The largely undeformed nature of the

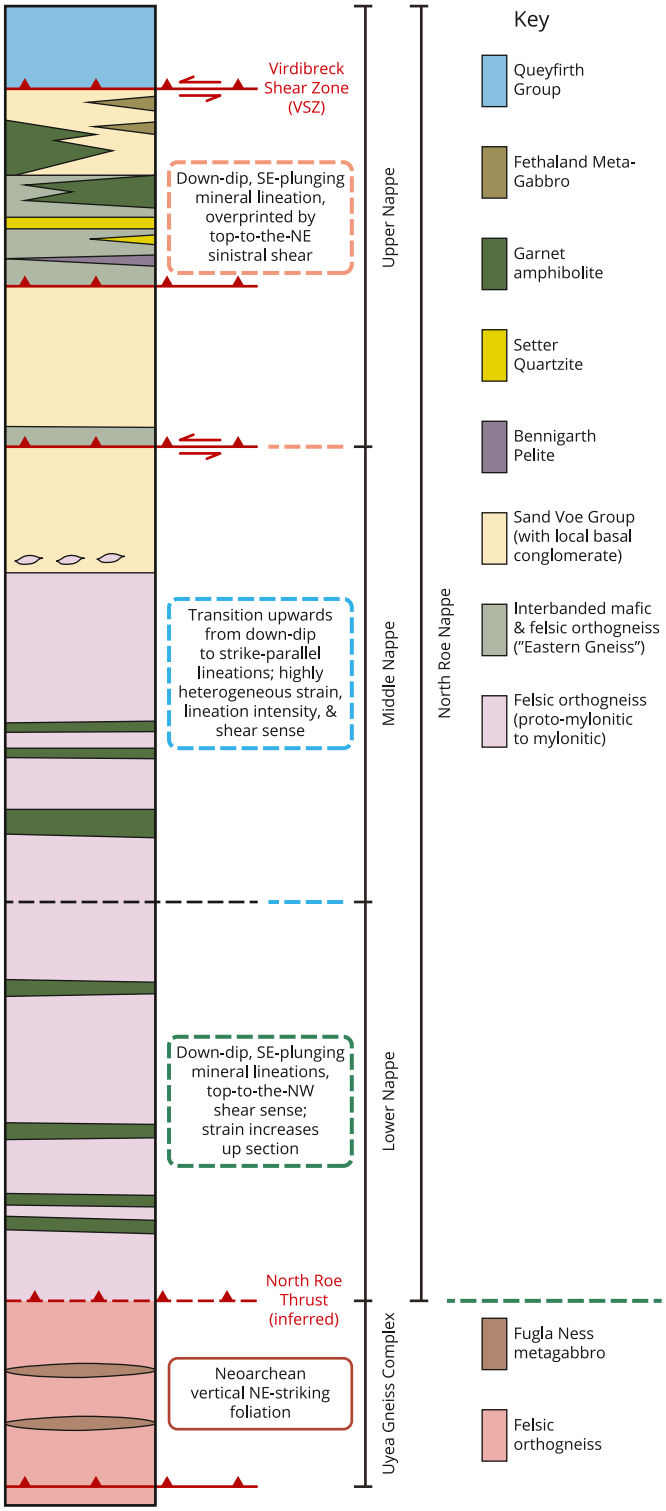

Fig. 2. Simplified tectonostratigraphic column for North Roe, showing the Lower, Middle and Upper nappes and their constituent lithologies. Modified from Pringle (1970), and Armitage (2021).

late-tectonic metagabbro bodies, and K-Ar and $^{40}Ar/^{39}Ar$ mineral ages of *c.* 2900–2500 Ma (Flinn et al., 1979) suggest that the UGC has not experienced any significant Palaeoproterozoic reworking. A similar dominance of Neoarchean protolith ages and absence of Palaeoproterozoic reworking is also seen in samples from a broad region of basement gneisses offshore to the west of Shetland (Holdsworth et al., 2019). The UGC and equivalent rocks offshore are assigned to the

Faroe-Shetland Terrane, which is interpreted as a continuation of the Archaean Rae Craton in NE Canada and Greenland (Holdsworth et al., 2019; Kinny et al., 2019).

The overlying North Roe Nappe is *c.* 3.6 km thick and is subdivided into three structurally distinct levels here termed the Lower (*c.* 1.1 km thickness), Middle (*c* 0.9 km thickness) and Upper (*c.* 1.6 km thickness) nappes (Fig. 1d and 2). The Lower North Roe Nappe comprises highly deformed orthogneisses thought to be the reworked equivalent of the footwall UGC (Pringle 1970; Kinny et al., 2019). The Middle North Roe Nappe comprises reworked UGC orthogneiss and part of the overlying Sand Voe Group which show a highly heterogeneous orientation, style and intensity of deformation. The Sand Voe Group - orthogneiss boundary (Fig. 1d and 2) is marked by a 200 m thick zone of mylonitic rocks known previously as the Wester Keolka Shear Zone (WKSZ; Pringle, 1970). Given that the Sand Voe Group has been compared with the Morar Group of the Moine Supergroup in mainland Scotland (Flinn 1985, 1988), it might follow that the WKSZ is the northern continuation of the Moine Thrust, which defines the western limit of Caledonian deformation on mainland Scotland and separates the foreland Lewisian Gneiss Complex from the Moine Supergroup (Fig. 1a; Andrews 1985; Ritchie et al., 1987; Flinn 1992, 1993). However, pebbles of epidote, K-feldspar and quartz are found within the Sand Voe Group, close to the contact with the UGC, suggesting that the boundary is a deformed unconformity and not a significant tectonic break (Fig. 2; Flinn et al., 1979; Walker et al., 2016).

Further east, the Upper North Roe Nappe comprises the Sand Voe Group interleaved with hornblendic- and quartzofeldspathic gneisses, termed the Eastern Gneiss (Fig. 1d and 2; Pringle 1970; Flinn 1988). The contact between the Middle and Upper nappes is marked by a thin but persistent slice of reworked orthogneissic basement and by significant changes in deformation style and metamorphic intensity (see below). Interleaved with the Eastern Gneiss are two metasedimentary units, the Bennigarth Pelite and the Setter Quartzite (Fig. 2; Flinn 1988). Modern isotopic dating has yet to be undertaken on the Eastern Gneiss and hence its protolith age is uncertain. It was initially viewed as orthogneissic basement to the Sand Voe Group on the basis of K-Ar and $^{40}Ar/^{39}Ar$ mineral ages of *c.* 2300-1000 Ma (Flinn et al., 1979; Flinn 1988), but U-Pb zircon data are required to confirm this interpretation. At structurally higher levels to the east, the Sand Voe Group is intruded by the Fethaland Metagabbro (Fig. 1d and 2) of unknown protolith age. The Queyfirth Group forms the uppermost part of the Upper Roe Nappe (Fig. 1d and 2). It is separated from the Sand Voe Group by a *c.* 20–30 m thick zone of intensely sheared mica-schist, the Virdibreck Shear Zone (VSZ) (Pringle 1970). Lying offshore to the east, the WBF (Fig. 1d), forms the eastern boundary of the Upper North Roe Nappe.

To the south, and cross-cutting the UGC and the North Roe Nappe is the Ronas Hill Granite, which is part of the Northmavine Complex (Fig. 1b–d; Mykura et al., 1976). U-Pb zircon dating of the Ronas Hill Granite by Lancaster et al. (2017) yielded a 427.5 ± 5.1 Ma intrusion age. This granite cuts across all ductile foliations in the country rocks and is post-tectonic (Lancaster et al., 2017).

2. Methods

2.1. Fieldwork, structural analysis and kinematic framework

Conventional geological field techniques employed included the collection of detailed primary field observations and structural information (e.g. foliation, fault information, kinematics, fold orientation, lineations, shear sense criteria, strain type and intensity, cross-cutting relationships). Other than the far western region of the UGC, the foliation in the study area has a fairly consistent strike and dip across the entire area (Fig. 3i–vii). Lineations and shear sense criteria are markedly variable requiring a consistent kinematic framework to be used relative to the strike and dip of the regional foliation (Fig. 4a). The terminology used here looks down onto the foliation plane and the terms 'clockwise' or 'anticlockwise' refer to the direction a lineation rotates as the viewer moves structurally up-section in successively exposed foliation planes (e.g. Fig. 4b).

Strain intensity was assessed qualitatively in the field based on the degree of attenuation of the compositional banding in the gneisses and metasedimentary rocks and strength of local shape-preferred orientation fabrics. Lineation intensities are very variable, but cannot be used to estimate strain intensity as rock fabrics vary from S, through L-S to local L > S tectonites (sensu Flinn 1965). Structural information was analysed using Stereonet 9.5 (Allmendinger et al., 2017).

2.2. Microscopy

Forty oriented hand specimens of deformed rocks were collected for optical microscopy and SEM analysis (BSEM, EBSD) of deformation textures, processes and crystallographic preferred orientations (CPOs). Thin sections were everywhere cut normal to the foliation and subparallel to the local mineral lineation in each sample (XZ kinematic plane; Passchier and Trouw 2005). The deformation temperature thermometer of Stipp et al. (2002) was used in optical thin sections to qualitatively estimate deformation temperatures. The thermometer predicts that at geological strain rates of $\sim 10^{-12}$ to 10^{-14} s^{-1} the dominant quartz microstructures evolve from: (1) grain boundary bulging recrystallisation (BLG; ~280–390 °C); to (2) subgrain rotation recrystallisation (SGR; ~420–490 °C); to (3) grain boundary migration recrystallisation (GBM; >530 °C) (See Appendix A). Below these temperatures, quartz is expected to display brittle behaviour, albeit with precursor dislocation creep-accommodated work hardening (Stipp et al., 2002). The quartz textures are then compared in the same samples to the feldspar deformation textures; this mineral is thought to dynamically recrystallise at temperatures of >450 °C (Tullis and Yund 1991; Stünitz and Fitz Gerald, 1993).

Quartz CPOs were measured on samples of deformed quartz veins/segregations from NW Mainland Shetland via Scanning Electron Microscopy (SEM), using Electron Backscatter Diffraction (EBSD). Samples were cut in the XZ plane (normal to foliation, parallel to local mineral stretching lineations). Further details of sample preparation, the acquisition and processing of EBSD data and the projections used to present CPO data are given in Appendix A.

3. Field relationships

The mostly E-W trending coastlines of North Roe (Figs. 1 and 3) expose an almost continuous across-strike outcrop (Figs. 2 and 5). Geological maps showing foliation and lineation (Fig. 3i–vii) and minor folding (Fig. 3viii–xiii) are presented, together with cross sections and local lineation swings (Fig. 5). The orthogneisses are cut by later steep, NE-SW and NW-SE trending brittle faults and the basal North Roe Thrust is obscured by one of these later normal faults (Fig. 1d and 5b). Detailed mapping shows that the strain orientation, type and intensity is markedly heterogeneous on a mesoscale (Fig. 5) with the Lower, Middle and Upper North Roe nappes showing different kinematic assemblages of structures. The boundaries between these domains are defined by changes of structural characteristics and/or interpreted deformational ages.

3.1. Uyea gneiss complex

The westernmost section of the UGC is mainly composed of coarse grained (>2 mm) granitic rocks and subordinate units of pegmatitic, intermediate and mafic compositions (Fig. 6a–e). Enclaves of mafic material show magma mixing textures within granodiorite suggesting a generally coeval age of formation before being crosscut by pegmatites (Kinny et al., 2019).

A variable intensity NE-SW vertical foliation (Fig. 3i and 6b, c) is defined by the alignment of micas and symmetrical lenticular augen of

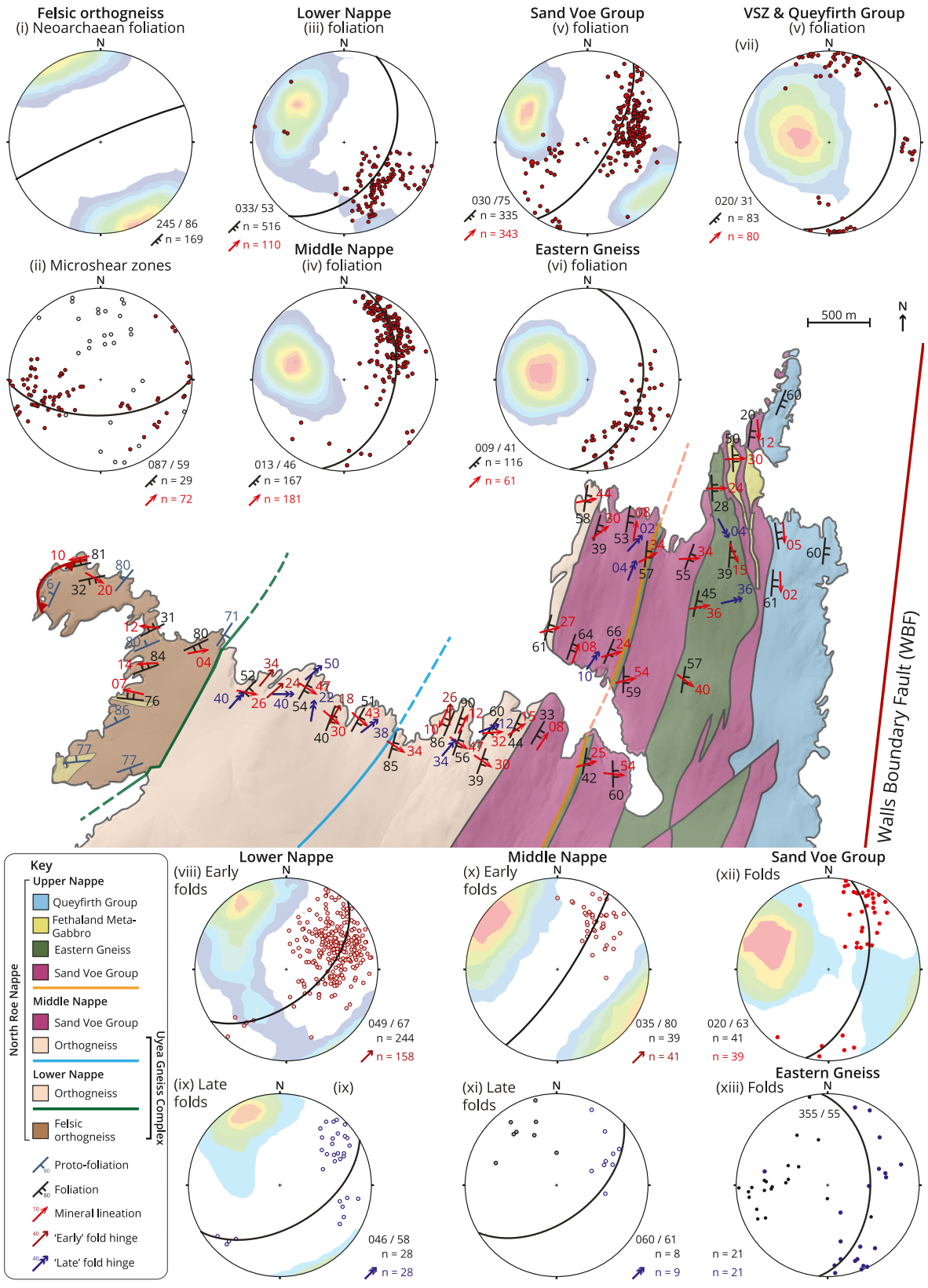

Fig. 3. **(a)** Geological map of North Roe showing foliation and lineations measurements. Stereonets display pole-to-plane contoured foliation, lineation and mean foliation plane (using right hand rule) for (i) 'Neoarchaean' foliation in foliated granodiorite; (ii) microshear zones in the Foliated granodiorite; (iii) Lower North Roe Nappe; (iv) Middle North Roe Nappe orthogneiss; (v) Sand Voe Group; (vi) Eastern Gneiss; (vii) VSZ and the Queyfirth Group. Stereonets viii-xiii display pole-to-plane contoured axial planes, fold hinges and mean axial plane for (viii) 'Early' folds in Lower North Roe Nappe, (ix) 'Late' folds in Lower North Roe Nappe, (x) 'Early' folds in Middle North Roe Nappe, (xi) 'Late' folds in Middle North Roe Nappe, (xii) Sand Voe Group, (xiii) Eastern Gneiss.

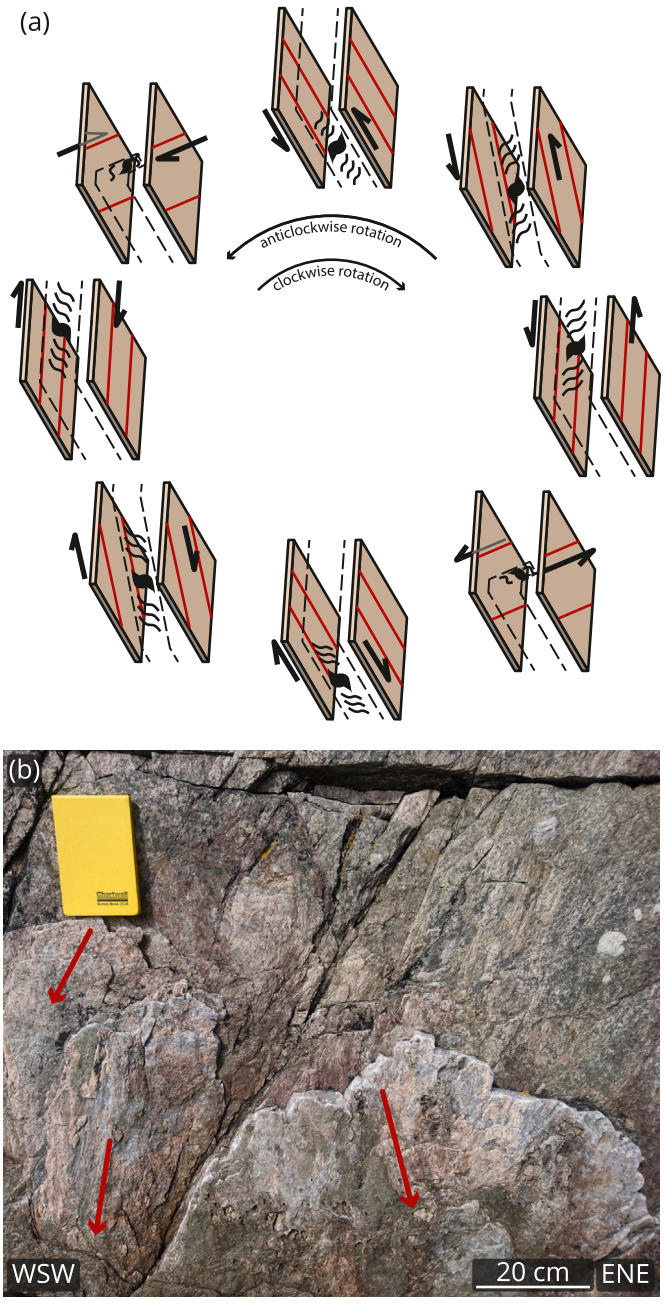

Fig. 4. **(a)** Kinematic compatibility during rotations of lineations and shear senses. **(b)** Photo showing an example of anticlockwise rotation in the field observed in a foliation plane-perpendicular view looking downwards (from HU 35074, 91713). In each successively higher foliation plane, the sense of lineation rotation is deduced relative to the lineation in the foliation planes below. Red lines show lineation orientations in three successive foliation planes (lowest to the left, highest to the right).

recrystallised feldspar and is considered to be of Neoarchaean age (Kinny et al., 2019). No associated mineral lineation is observed and finite strain is generally relatively low. Overprinting this foliation are anastomosing mylonitic shear zones typically 4–10 cm thick (Fig. 6d–f). Shear zones and their associated foliations are variable in orientation (Fig. 3ii) but are all generally associated with westerly-directed senses of tectonic transport based on preserved S-C-C' fabrics and asymmetrically sheared porphyroclasts (Fig. 6d–f). On the inaccessible western cliffs of the island of Uyea (Fig. 5a and 6f), a SE-dipping zone of highly deformed rock interpreted by us to be ultramylonite *c.* 15 m thick asymmetrically wraps m-scale bodies of amphibolite (UK Ordnance Survey Grid Reference HU 31090 93300). Elsewhere, N-S trending pegmatites cutting the gneisses display local top-to-the-north (sinistral) shearing along their margins (Fig. 6e) (HU 32620 92718).

3.2. Lower North Roe Nappe

The Lower North Roe Nappe (NRN) is separated from the UGC to the west by an inaccessible, vertical N-S striking, east-side-down brittle fault, that cross-cuts the ductile foliations in the adjacent rocks (HU 32714 92090) (Fig. 1d). Thus, the original boundary between the UGC and the Lower NRN is no longer exposed at the present-day surface (Fig. 5b).

Strain within the Lower NRN increases structurally up-section. In its lowest portion, pods of relatively undeformed gneiss, amphibolite and pegmatite are wrapped by the foliation (e.g. HU 33050 92170). Here, strain is concentrated along mylonitised lithological contacts, leaving adjacent areas of relatively low strain. At structurally higher levels in the east of the domain, a 200 m thick section shows intense schistosity and ultramylonitic textures. Foliations in the Lower NRN are NE striking and moderately SE dipping, with a down-dip SE plunging mineral lineation (Fig. 3iii). Shear bands, S-C fabrics and asymmetrically sheared feldspar porphyroclasts display top-to-the NW shear senses (Fig. 7a).

Two generations of folding occur in the structurally lowest levels of the domain. 'Early' micro- to meso-scale folds are tight to isoclinal and display curvilinear hinges that plunge shallow-to steeply NE or SW with SE-dipping axial planes and overall NW to NNW vergence (Figs. 3viii and 7b); eye structures are locally preserved (Fig. 7c). 'Late' folds are generally open to tight, meso- to macro-scale features (Fig. 7d) and refold local 'Early' folds, lineations and shear sense indicators (e.g. hence the WNW dip of the structures shown in Fig. 7a). 'Late' folds are characterised by shallow to moderately NE plunging fold hinges (Fig. 3ix). Axial planes dip steeply to the SE and folds mostly show NW vergence. (e.g. HU 33300, 92188).

3.3. Middle North Roe Nappe

The Middle NRN is best exposed in two northerly-facing coastal sections: a northern section east of Garmus Taing (Figs. 1 and 8a) and the southern section eastwards from Grut Ness (Figs. 1 and 8b). In both sections, the lower part of the nappe is made up of reworked UGC orthogneisses, whereas the upper part comprises metasedimentary rocks of the Sand Voe Group (Figs. 2 and 8). Although the foliation dips consistently moderately to steeply SE (Fig. 3iv, v), the strain intensity (orthogneiss to protomylonite to ultramylonite), lineation intensity and orientation and the associated shear senses are extremely variable on metres to tens of metres scales (Fig. 8a and b). This leads to the preservation of a stack of foliation-parallel domains with different structural characteristics and kinematics (Figs. 8 and 9). Overall, strain increases eastwards and up section culminating in a c. 200–300 m thick belt of ultramylonite at the orthogneiss – Sand Voe Group contact (Figs. 5 and 8a, b; the 'Wester Keolka Shear Zone' of Pringle 1970). Furthermore, a transition from down-dip to strike-parallel lineations occurs from the base to the top of the Middle NRN (Figs. 8a, b and 9).

In both coastal sections, there are domains where lineations plunge down the dip of the local foliation and shear criteria indicate *either* top-to-the-NW thrusting *or* top-to-the-SE extension (Fig. 8a–c, f). These are interleaved with domains where lineations are parallel to the local foliation strike and are associated with *either* top-to the-NE sinistral *or* top-to-the-SW dextral shear criteria (Fig. 8a, b, d, e). Two types of transition are preserved that separate these end-member kinematic domains:

i) kinematically compatible **asymmetric transitions** where gradual rotation of lineations and shear sense occurs continuously clockwise or anticlockwise, leading to intervening domains of obliquely

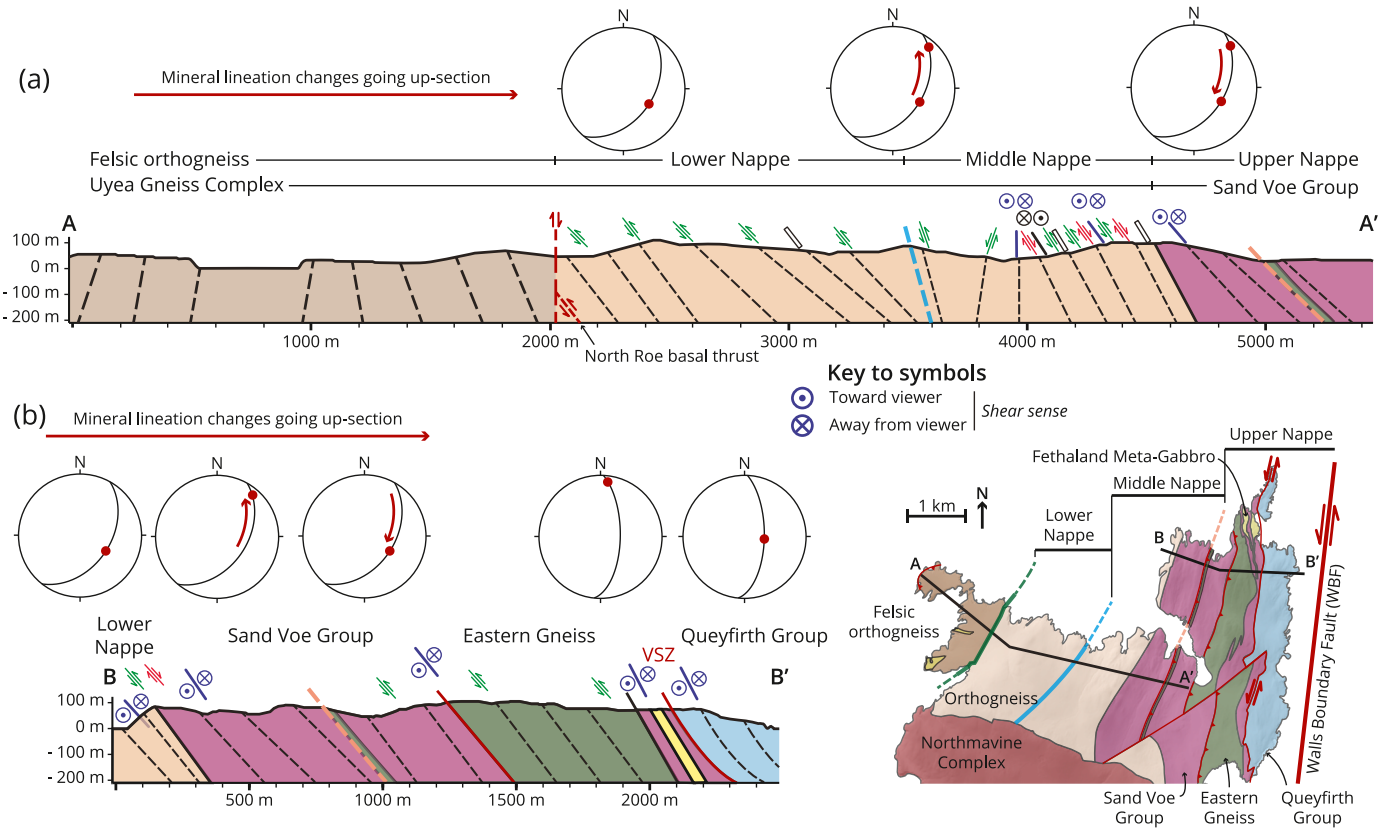

Fig. 5. Geological cross sections A-A′ and B-B′ (locations in inset map) showing main structural domains, domain bounding faults and foliation. Kinematics, noted by colour and shear arrows, coaxial deformation, noted by a white rectangle, and representative lineations in stereonets are also shown.

plunging lineations and intermediate shear senses (e.g. Fig. 4a and b, HU 35918 93773); and

ii) schistose **symmetric transitions** where mylonitization is typically more intense, lineations are weak or absent and shear criteria are absent; these appear to represent domains of predominantly coaxial strain, with the schistose deformation typically sandwiched between horizons of antithetic (opposed) shear senses (e.g. Fig. 9; HU 35980 93773).

It is important to emphasise that in most of the Middle NRN, there is no field evidence for overprinting of lineations in different orientations or shear senses. Although the various kinematic horizons mapped can be traced along strike on a decimetre-scale (as indicated in Fig. 8a and b), kinematic horizons cannot be precisely correlated along strike on more regional scales. However, the presence of kinematically compatible asymmetric and schistose symmetric transitions in both outcrops suggests that these domains are not localised features and represent a common characteristic of deformation throughout the Middle NRN.

The foliation in the overlying psammites, semi-pelites and garnet mica schists in the Sand Voe Group strikes NE-SW and dips moderately to the SE (Fig. 3v). Close to the contact with the orthogneisses, lineations plunge shallowly NNE at low angles to strike (Fig. 3v). In the well exposed Grut Ness section, flattened quartz, K-feldspar and epidote pebbles (1–5 cm across) are preserved within 1–2 m of the orthogneiss-metasediment contact and seem to indicate the presence of a sheared unconformity and sparse basal conglomerate (Fig. 10a; HU 35543 91864). Psammites and mica schist located close to this contact have an intense blastomylonitic schistosity, but only a weakly developed mineral lineation, suggesting strain within the oblate field ($1 > k > 0$; sensu Flinn 1962). Sporadic shear-sense indicators (asymmetric porphyroclasts) suggest top-to-the NE (sinistral) displacements close to the contact (Fig. 10a), but despite being highly deformed, much of the Sand Voe Group in the Middle NRN preserves few kinematic indicators (Figs. 8 and 9).

Minor and meso-scale folds in the Middle North Roe Nappe are uncommon and are mostly developed in less-deformed pegmatite and amphibolite bodies. In the deformed pegmatites, occasional tight to isoclinal meso-scale folds verge NW and display gently NE plunging hinges, with inclined axial planes dipping SE (Fig. 3x). In large amphibolite bodies, open to tight, NE-plunging meso- to macro-scale fold pairs refold foliations and associated mineral lineations, suggesting a 'Later' age of formation (Fig. 3xi).

3.4. Upper North Roe Nappe

3.4.1. Sand Voe group

In the western part of Fethaland and either side of Sand Voe (Fig. 8), the lower boundary of the Upper North Roe Nappe separates more highly deformed mylonitic Sand Voe Group from less deformed equivalent rocks in its hangingwall. It is marked by a continuous, up to 50 m thick slice of highly deformed mafic orthogneiss (e.g. HU 3585 9130) similar in lithology to the Eastern Gneiss seen further to the east (see below). The foliation in the Upper Roe Nappe strikes NE-SW and dips moderately to the SE (Fig. 3v). Moving up-section (west to east), mineral lineations rotate clockwise over a distance of several hundred metres from gentle NNE plunges to down-dip along the contact with the overlying Eastern Gneiss (Fig. 3v–vi).

Only one generation of micro to meso-scale folding is observed in a series of psammitic horizons with a total thickness of *c.* 50 m (Fig. 10b and c; HU 36241 92307). Folds of compositional layering and quartz veins are tight to isoclinal and upright to inclined. Hinges plunge shallowly to moderately NE, parallel to local lineations, while axial planes and cleavage strike NNE and dip moderately to steeply ESE (Fig. 3xii). An axial planar cleavage is common, defined by an alignment of micas

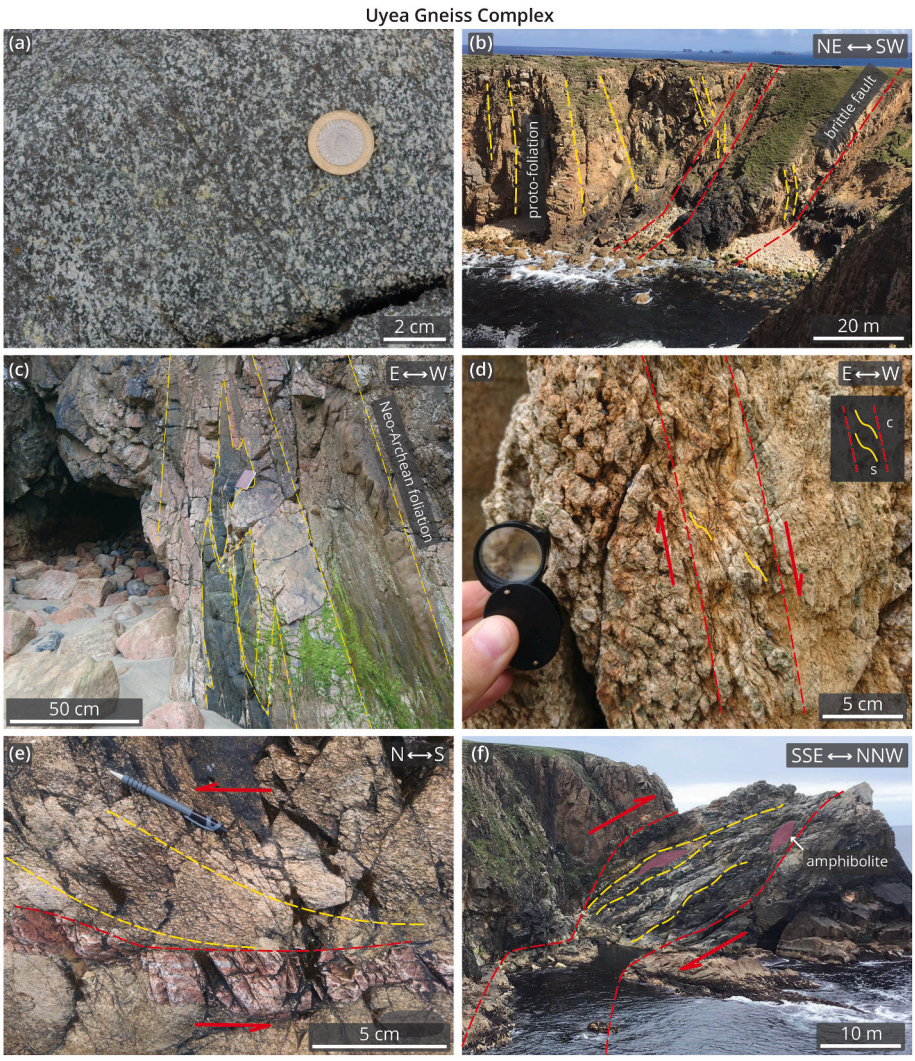

Fig. 6. Field photographs from the UGC of **(a)** subordinate metagabbro (HU 31122, 91339). **(b)** Vertical foliation in acid orthogneisses cross-cut by vertical NW-SE trending post-Caledonian brittle faults (in red; HU 31837, 92252). **(c)** Steeply dipping 'Neoarchaean' foliation (in yellow) overprinting mafic and felsic material which show magma mixing textures (HU 32017, 92580). **(d)** 'Neoarchaean' foliation in a foliated granodiorite crosscut by a microshear zone showing top-to-the-W shear sense (HU 32620, 92718). **(e)** Weakly foliated pegmatitic dyke (pink colour) showing sinistrally sheared margins (HU 31937, 92718). **(f)** c. 15 m thick shear zone on inaccessible cliff face on Uyea's western coastline showing SE-dipping foliation wrapping m-scale lenses of amphibolite and top-to-the NW shear sense (HU 31090 93300).

parallel to fold axial planes, which is subparallel to the regional foliation (Fig. 10c). Where defined by quartz veins, local foliations may wrap or be slightly discordant to fold hinges (Fig. 10b). Occasionally within less deformed and more competent psammitic horizons, a lamination oblique to the main compositional banding defined may represent relicts of cross bedding (HU 36270 91425). Collectively, these observations suggest that the folded psammitic horizons represent regions of lower strain.

The foliation becomes mylonitic in the upper portions of the Sand Voe Group close to the contact with the Eastern Gneiss. Up to 30 cm long quartz rods are developed there (Fig. 10d). These plunge down-dip to the E and are associated with a top-to-the W S-C shear fabric (Fig. 10e). However, in a few locations, a strike-parallel, top-to-the-N (sinistral) S-C shear overprints the quartz rods and cross-cuts the top-to-the W shearing shear fabric (Figs. 10f and 11). This overprinting relationship suggests an 'early' and 'late' age relationship respectively between top-to-the-W thrusting here and top-to-the N (sinistral) shear in the Eastern Gneiss and upper parts of the Sand Voe Group.

3.4.2. *Eastern gneiss*

The Eastern Gneiss comprises interlayered mafic and felsic units, each up to 10–30 m thick, with a series of sheared garnet-pyroxene-amphibole ultramafic lenses *c.* 0.5–2 m long (e.g. Fig. 11a). These are especially common close to the contact with the underlying Sand Voe Group (e.g. HU 37205 93560). Wrapping ultramafic lenses are sheared mafic units of garnet-mica-hornblendic gneiss interlayered with quartzofeldspathic gneiss (Fig. 11a). Felsic components are quartzofeldspathic meta-igneous material, garnet-mica schist and feldspathic quartzite metasediments, including two distinctive marker horizons, the Bennigarth Pelite and Setter Quartzite (Pringle 1970; Figs. 2 and 11b). The lower parts of the Eastern Gneisses are predominantly schistose mylonitic rocks, and strain generally decreases up section and eastwards until only a weak or no internal fabric is preserved, particularly in amphibolites (HU 37418 93507). Strain then increases again upwards to the upper Eastern Gneiss-Sand Voe Group contact which is pervasively mylonitised and carries numerous 1 cm thick quartz veins.

Foliation across the Eastern Gneiss strikes N-S and dips moderately to gently to the E (Fig. 3vi). Near the underlying contact with the Sand Voe Group and throughout much of the Eastern Gneiss, lineations plunge

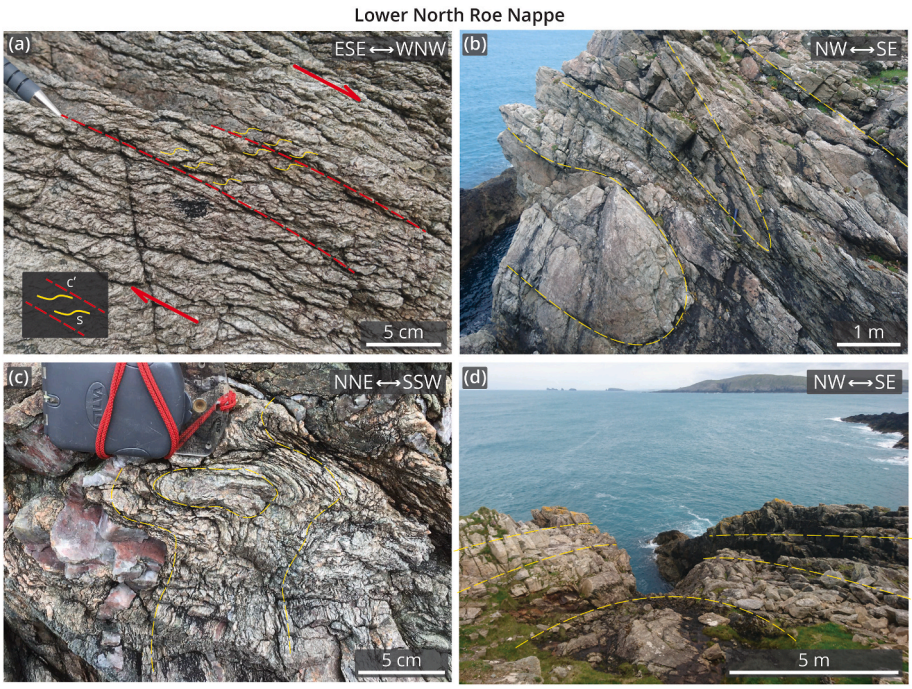

Fig. 7. Field photographs of the Lower North Roe Nappe. (**a**) Top-to-the-NW S-C′ shear fabric found in the WNW-dipping limb of a 'Late' fold (HU 33403, 92236). (**b**) Tight to isoclinal, inclined, meso-scale 'Early' folds showing NW vergence (HU 33440, 92244). (**c**) Micro-meso scale 'Early' sheath fold showing eye structure (HU 33041, 92162). **(d)** Macro-scale, open, inclined, gentle 'Late' fold (HU 33725, 91903).

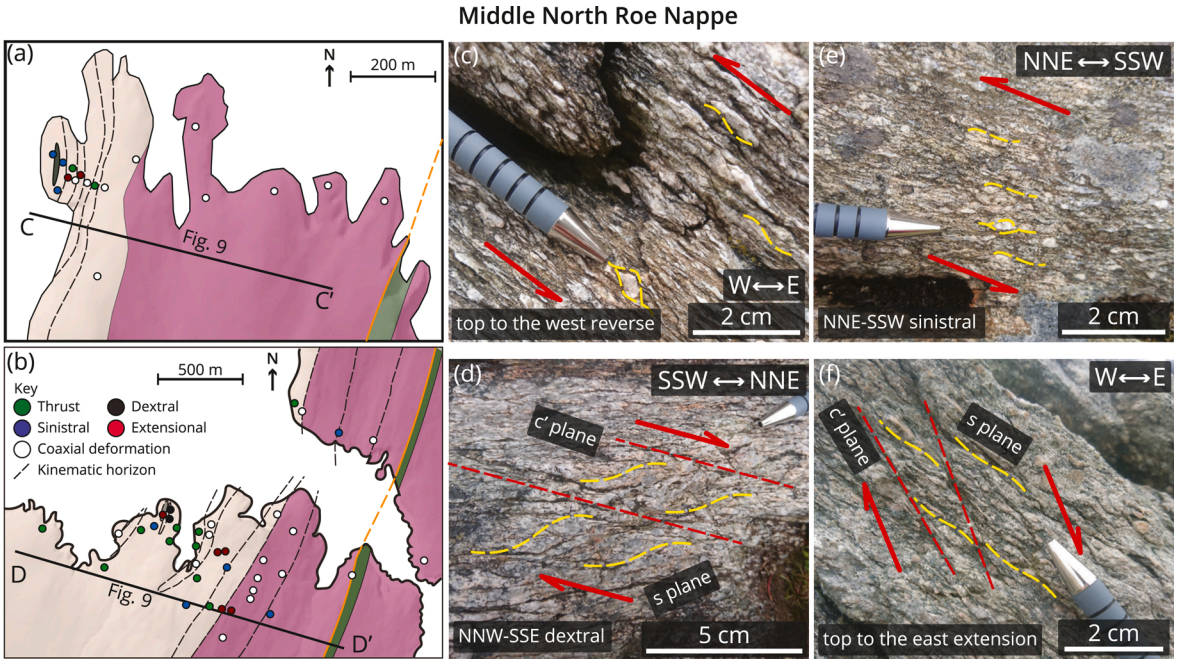

Fig. 8. Structural maps and field photographs of the Middle North Roe Nappe detailing the shear sense, foliation and lineation observed in the field. Horizons of similar kinematics are grouped into domains (dashed lines) that strike parallel to foliation. (**a**) Northernmost exposure. (**b**) Southernmost exposure of the Middle North Roe Nappes. Lines of Sections C-C′ and D-D′ shown in Fig. 9 are also indicated. (**c**) Top-to-the-W thrust shear (section view, HU 34914, 91879). (**d**) Strike-parallel dextral shear (plan view, HU 35945, 93700). (**e**) Strike-parallel sinistral shear (plan view, HU 35046, 91259). (**f**) Top-to-the-E, down-dip extensional shear (section view, HU 35954, 93736).

down-dip to the E and are accompanied by top-to-the W thrusting kinematic indicators (Fig. 11c–d, HU 37250 94230). However, sporadically throughout the Eastern Gneiss and along the upper and lower Sand Voe Group contacts, a top-to-the N shear sense is also observed which overprints the top-to-the W thrust shear sense. Foliation strike-parallel lineations accompanying the top-to-the N shear are present, but are mostly poorly developed.

Folds, defined by gneissic banding, are rare and are best preserved in a mafic horizon within the upper part of the Eastern Gneiss (HU 37248 94209). Folds are typically meso- to micro-scale, open to tight and upright (e.g. Fig. 11e). Fold hinges are highly curvilinear, plunge shallowly to steeply on a N-S girdle (Fig. 3xiii) and verge generally west. Axial

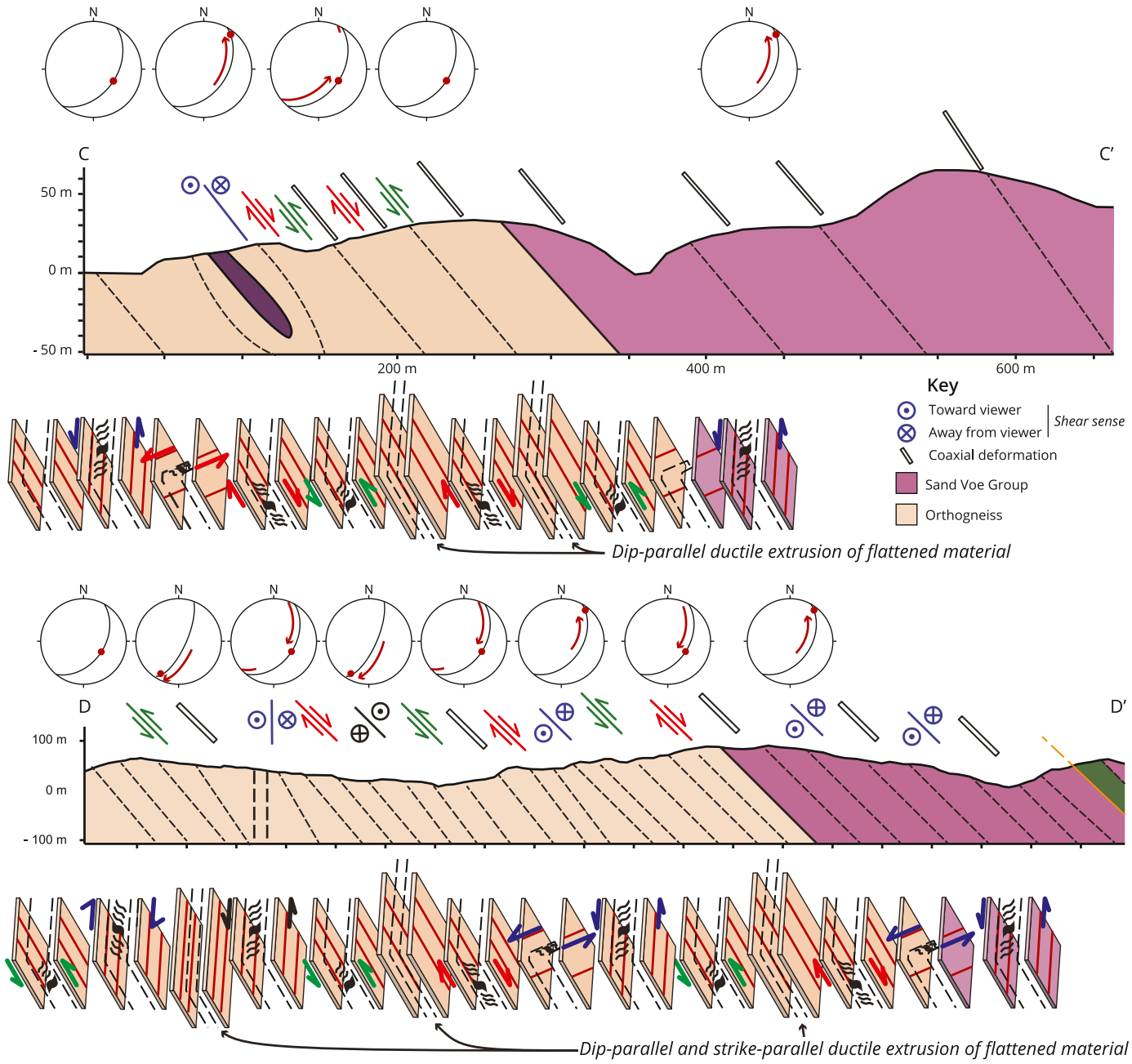

Fig. 9. Geological cross sections showing the change of lineations and shear sense between domains in the Middle North Roe Nappe. Above each cross section, the changes in mineral lineations moving up-section are shown. Below are panel diagrams of the shear senses observed on the cross section. Note that coaxially-deformed horizons show *both* dip-parallel and strike-parallel stretching locally.

planes strike N-S and dip moderately E.

3.4.3. Fethaland Metagabbro

The Fethaland Metagabbro, located within the upper part of the Sand Voe Group, extends for *c.* 300 m along strike and is in places almost 100 m thick. The body is medium grained and composed of fine grained (1–2 mm) garnet, plagioclase, hornblende with retrogressive actinolite and chlorite. The sharp contact of the metagabbro with the Sand Voe Group is everywhere concordant with foliation and highly deformed (HU 37290 94215). A moderate to weak foliation is developed in the metagabbro, striking N-S and lying parallel to foliation in the Sand Voe Group. In local regions of low strain, the metagabbro preserves an original magmatic ophitic texture (Fig. 11f, HU 37320 94280). Replacing hornblende are fibrous green mats of actinolite and/or chlorite. A mineral lineation defined by weakly aligned plagioclase shows a dip-parallel, E plunge, which is oblique to the regional mineral lineation observed in adjacent parts of the Sand Voe Group and in the overlying VSZ. No shear sense or folding is observed in the metagabbro.

3.4.4. The Queyfirth group and Virdibreck shear zone

The Queyfirth Group comprises interbanded garnet-mica schists, psammites and metamorphosed basaltic tuffs (amphibolites) with occasional lenses of sheared ultramafic material (Figs. 2 and 12). Grain sizes in the Queyfirth Group are relatively coarse (>1 mm) and the rocks are mostly not mylonitised, suggesting lower finite strains compared to most of the underlying sequences to the west (Roper, 1972). Early garnets are widely replaced by chlorite and amphiboles are extensively retrogressed to chlorite and epidote.

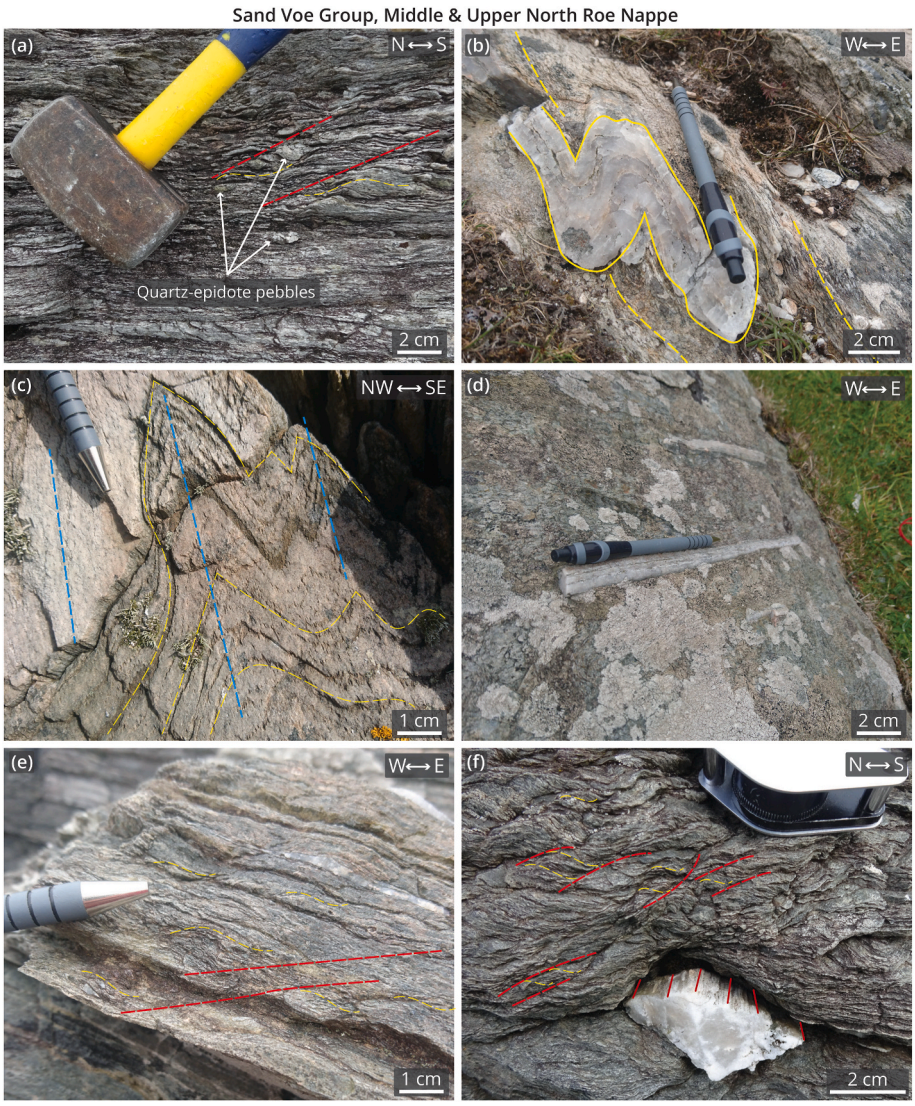

Fig. 10. Summary of structures observed in the Sand Voe Group. (**a**) Top-to-the N S-C shear fabric close to the Sand Voe Group-orthogneiss contact (WKSZ) (HU 35543 91864). (**b**) Tightly folded quartz vein verging W (HU 36241 92307). (**c**) Tight-to-isoclinal folds in lower-strain psammitic horizons with strong axial planar cleavage (HU 36241 92307). (**d**) Intensely deformed horizon showing a strong schistosity and elongate quartz rods plunging down-dip to the E (HU 37094 93788). (**e**) Top-to-the W S-C shear fabric associated with rocks shown in d) (HU 37081 93770). (**f**) Quartz rods that plunge to the E overprinted by a top-to-the N S-C′ fabric (HU 37094 93788). Note that (a) lies in Middle NRN, (b–f) are in the Upper NRN.

Marking the contact between the Sand Voe and Queyfirth groups is the Virdibreck Shear Zone (VSZ; Fig. 1d and 2), which is composed of sheared chlorite-bearing pelites derived from Queyfirth Group protoliths. At the Point of Fethaland (HU 3750 9440), foliation in the VSZ strikes N-S and dips gently E (Fig. 3vii). However, along strike and to the south at Isbister (HU 37380 91720) the VSZ shows a NNE-SSW strike and a steep ESE or sub-vertical dip (Fig. 13a). Both localities show a gently plunging strike-parallel lineation (Fig. 3vii) with top-to-the N/NNE (sinistral) shear senses (Fig. 12a and b).

The foliation in the overlying Queyfirth Group in both Fethaland (Fig. 3vii) and the Queyfirth Peninsula (Fig. 13ai) strikes N-S and dips moderately to steeply E. A sparsely developed down-dip E plunging lineation is found in schists, associated with S-C and S-C' shear fabrics denoting top-to-the W shear senses. Occasional cm-scale, tight to isoclinal, chaotic folds with variable NE-SW to NW-SE plunging hinges are found in the metamorphosed basaltic tuffs.

Two sets of folds in the Queyfirth Group are best seen in the Queyfirth peninsula to the south (Fig. 13aii, iii; see also Armitage et al., 2021). 'Early' folds are micro- to meso-scale, tight to isoclinal and verge W (Fig. 12c). Fold hinges plunge gently S and axial planes strike N-S (Fig. 13aii). Such 'Early' folds are widely developed throughout the Queyfirth Group (Armitage et al., 2021) and are thought to be part of a regional fold set. 'Later' folds are micro- to meso-scale, open to tight kink folds with 'Z' shaped dextral vergence (Fig. 12d). Fold hinges are variable in plunge, but the majority are steep to vertically plunging with axial planes that strike N-S (Fig. 13aiii). 'Later' folds are well developed in pelitic horizons proximal to areas of brittle faulting, suggesting that 'Later' folds and brittle faults formed simultaneously. The faults typically carry mm to cm thick, grey phyllosilicate-rich gouges. They strike NE-SW and steeply dip SE, or NW-SE and dip SW (Fig. 13aiv). Slickenlines and S-C shears within the fault gouge show dextral shear senses on NE-SW faults and reverse shear senses on NW-SE faults. No cross-cutting relationships can be determined between these fault sets which are therefore considered to have formed simultaneously.

3.5. *Quartz veins and segregations*

Variably – and often highly – deformed quartz veins and segregations are very common throughout the North Roe Nappe (e.g. Figs. 7c and 10b,d, f). They give an opportunity to study deformation textures and

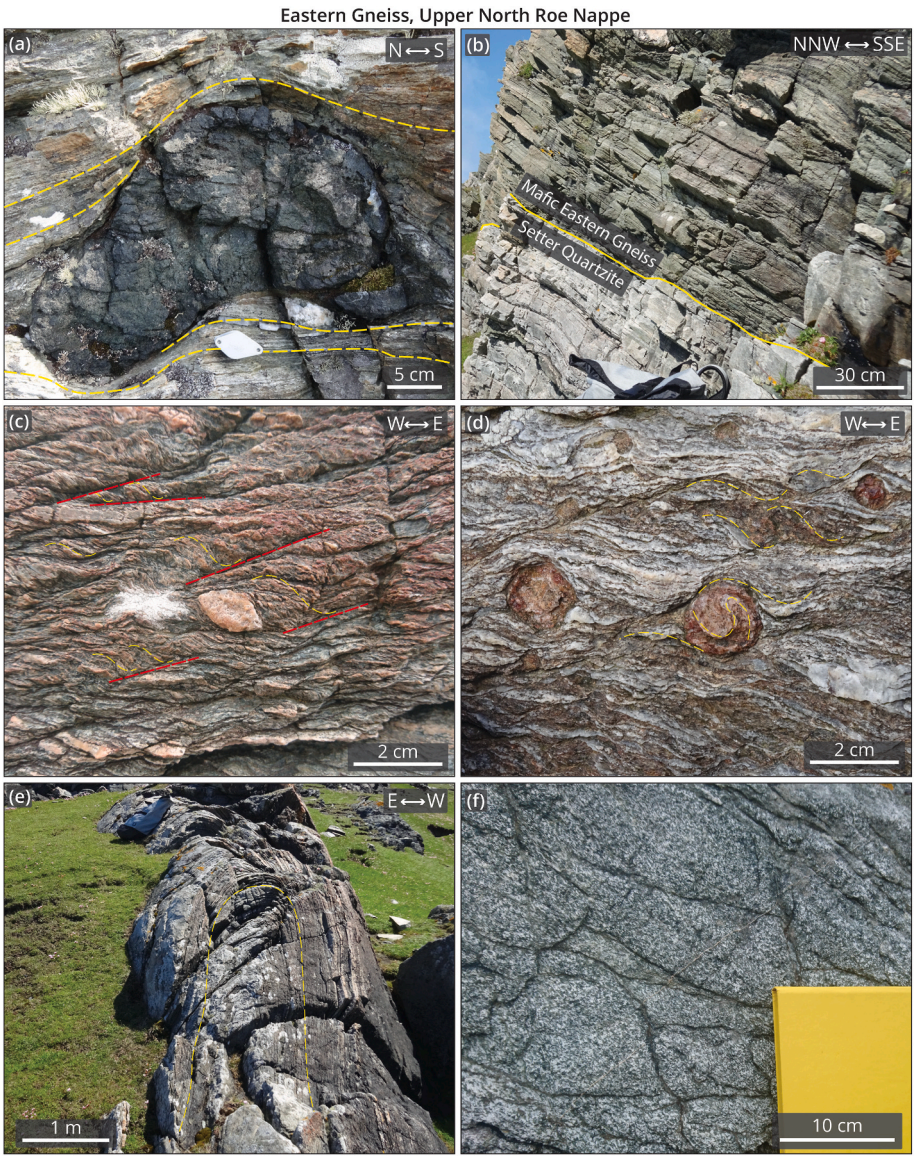

Fig. 11. Structures in the Eastern Gneiss and Fethaland Metagabbro, Upper NRN. (**a**) Sheared ultramafic lens wrapped by mafic material (HU 37205 93560). (b) Contact between the felsic Setter Quartzite and a mafic component of Eastern Gneiss (HU 37205 93560). (**c**) Top-to-the W S-C′ fabric (HU 37250 94230). (**d**) Rotated garnets and S-C fabric showing top-to-the W shear, Bennigarth Pelite (HU 37250 94230). (**e**) Tight meso-scale fold (HU 37250 94230). (**f**) Fethaland Metagabbro showing low strain and chloritization (HU 37248 94209).

carry out EBSD analyses of crystallographic preferred orientation fabrics in units that are essentially monomineralic (e.g. see Lloyd 2020). Where possible, quartz veins were sampled from each tectonic unit across the North Roe Nappe (Fig. 13b). Further samples were taken from areas of specific interest where changes in kinematics, strain state or strain type occurred. All samples collected were composed almost entirely of quartz (99–100%) with small amounts of chlorite and muscovite. Note that most of the veins studied formed relatively early in the preserved deformation history and so are assumed here to have experienced a substantial proportion of the deformation history recorded in the adjacent host rocks.

3.5.1. Lower North Roe Nappe

In the Lower NRN, quartz veins are generally uncommon in the lowest, westernmost portion of the domain. However, those found to the east on a sheared orthogneiss-ultramylonite contact occur in 2–3 m thick rock domains that show 50% by volume of quartz veins (sample TA18-14.A). Quartz veins are individually 2–4 cm thick, up to 20 cm long and lie parallel to local foliation. On quartz vein surfaces, clearly defined quartz-rod mineral lineations are consistently orientated parallel to the local mineral lineation in the surrounding host rocks. Also occurring locally are horizons of intense quartz veining along pegmatite-orthogneiss contacts. Sample TA18-84 was taken *c.* 200 m from the Lower-Middle nappe boundary, proximal to an area of protomylonite. Here, quartz veins occur sporadically and are 2 cm thick and 10 cm long.

3.5.2. Lower and middle north Roe Nappe

Quartz veins are distributed heterogeneously in the Middle NRN. At its base, quartz veins are sparse becoming more common up sequence. Veins occur along contacts between: top-to-the NW and sinistral shear domains (HU 34695 91750, sample TA18-86; N-S dextral shear and top-to-the W shear domains (HU 34888 91891); schistose units lacking shear sense and top-to-the W shear horizons (HU 35095 91790); top-to-the W and top-to-the E shear domains (HU 34843 91340, sample TA19-37); and the orthogneiss-Sand Voe Group boundary (HU 35405 91476, sample TA19-29). All of these contacts have a higher density (≥50% area) of quartz veins compared to other regions. In these areas, quartz veins are typically 1–5 cm thick and up to 30 cm long. Veins lie sub-

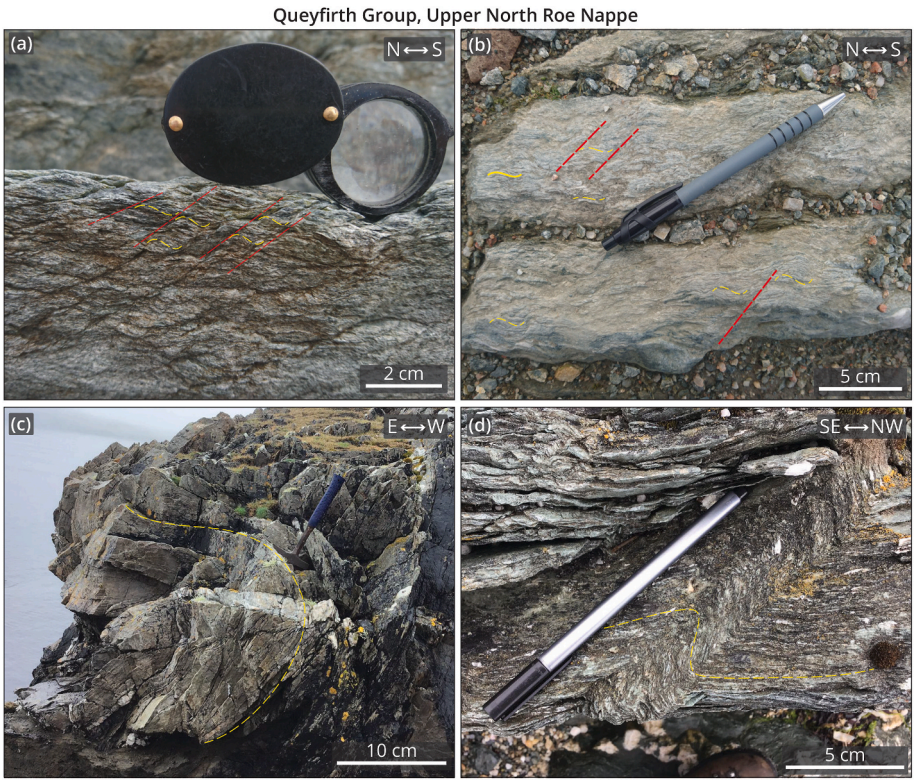

Fig. 12. Structures observed in the Queyfirth Group and the VSZ on Fethaland and Queyfirth Peninsular, Upper NRN. (**a**) Top-to-the-N shear sense on the VSZ on the Point of Fethaland (HU 3750 9440). (**b**) Sinistral N-S shear sense on the VSZ at Isbister (HU 3750 9440). (**c**) W-verging, tight and overturned 'Early' fold in a psammitic horizon of the Queyfirth Group on the Queyfirth Peninsular (HU 37201 82578). (**d**) 'Z' shaped dextrally verging 'Late' fold in the Queyfirth Group on the Queyfirth Peninsular (HU 37201 82578).

parallel to foliation, are sheared and display strong quartz rodding parallel to local host rock lineations. Where folding is present, quartz veins are usually folded.

A broader swarm of quartz veins (≥30% area) occurs from the orthogneiss-Sand Voe Group contact to *c.* 300 m structurally up-section (samples TA19-14, TA19-17). Here quartz veins are between 3 and 5 cm thick, *c.* 25 cm long, lie parallel to foliation and display strong quartz rodding parallel to strike and local lineations. In a low-strain folded psammitic part of the Sand Voe Group (HU 36241 92307), quartz veins define tight-isoclinal folds that plunge NNE with axial planes subparallel to the shear surface. In the upper part of the Sand Voe Group proximal to contact with the Eastern Gneiss and on the Queyfirth Peninsula, quartz veins are less common (1 vein per 2 m). Veins are *c.* 2–3 cm thick and 10–20 cm long and show mineral lineations parallel to local lineations (samples TA19-11, TA19-12, TA19-50).

3.5.3. Virdibreck shear zone

Within the VSZ, quartz veins are common (2 per 1 m, samples TA19-23, TA18-33), 1 cm thick and 5–10 cm long. Veins lie flattened parallel to foliation and slightly oblique to the S plane of associated S-C shear fabrics. On vein surfaces, a mineral lineation parallel to strike is clearly defined.

4. Microstructures and textures

In this section we describe optical and SEM electron backscattered diffraction (EBSD) microscopy analyses of samples from the field area. In general, optical microscopy was used to constrain sample mineralogical and microstructural relationships (Figs. 14–18) and, where possible, to interpret temperature and/or metamorphic facies conditions within a relative deformation chronology. In addition, EBSD analysis (Fig. 19a–k) was used to investigate quartz petrofabrics. Data gleaned from (EBSD-derived) quartz c-axis pole plots can be used to determine shear-sense, constrain the style of 3D strain, including its k value (Flinn, 1962), show the orientation of kinematic vorticity axes and bracket deformation temperature (e.g. Wallis, 1992, 1995; Law et al., 2004; Law, 2014; Passchier and Trouw, 2005; Faleiros et al., 2016).

We present the orientations of quartz <0001> c axes collected using EBSD analyses (step sizes ~5 mm) of foliation-normal, lineation-parallel thin sections of quartz veins/segregations (see Fig. 13a and b for localities). MTEX, an open-source MATLAB toolbox (Bachmann et al., 2010; https://mtex-toolbox.github.io/), was used to produce grain orientation maps and c-axis pole plots (Fig. 19a–k, columns 1–2). EBSD analysis can also be used to distinguish dynamically recrystallised (i.e. 'low' strain) grains from relict (i.e. 'high' strain) grains via the method proposed by Cross et al. (2017). This method quantifies the degree of intracrystalline lattice distortion in each grain, which is proportional to dislocation density, and can be visualised in terms of the misorientation angle between every pixel in a grain and the mean orientation of that grain (so-called 'mis2mean', Fig. 19a–k, column 3). The average 'mis2mean' defines the 'grain orientation spread' (GOS) value of each grain and acts as a measure of the distortion, providing a proxy for dislocation density. A threshold GOS value separates recrystallised and relict grains (Fig. 19a–k, column 4), from which mean grain sizes for both fractions can be estimated. Based on this approach, Cross et al. (2017) derived a recrystallised grain size palaeopiezometer $s_{1\text{-}3} = (10^{3.91\pm0.41}/D_{RMS})^{1/1.41\pm0.21}$, where $s_{1\text{-}3}$ is differential stress and D_{RMS} is the root mean squared recrystallised grain size. All samples provided D_{RMS} values and hence estimates of differential stresses (Fig. 19a–k, column 5), from which, depending on temperature, indications of deformation strain-rates can be made via substitution into appropriate constitutive equations (e.g. Lusk et al., 2021).

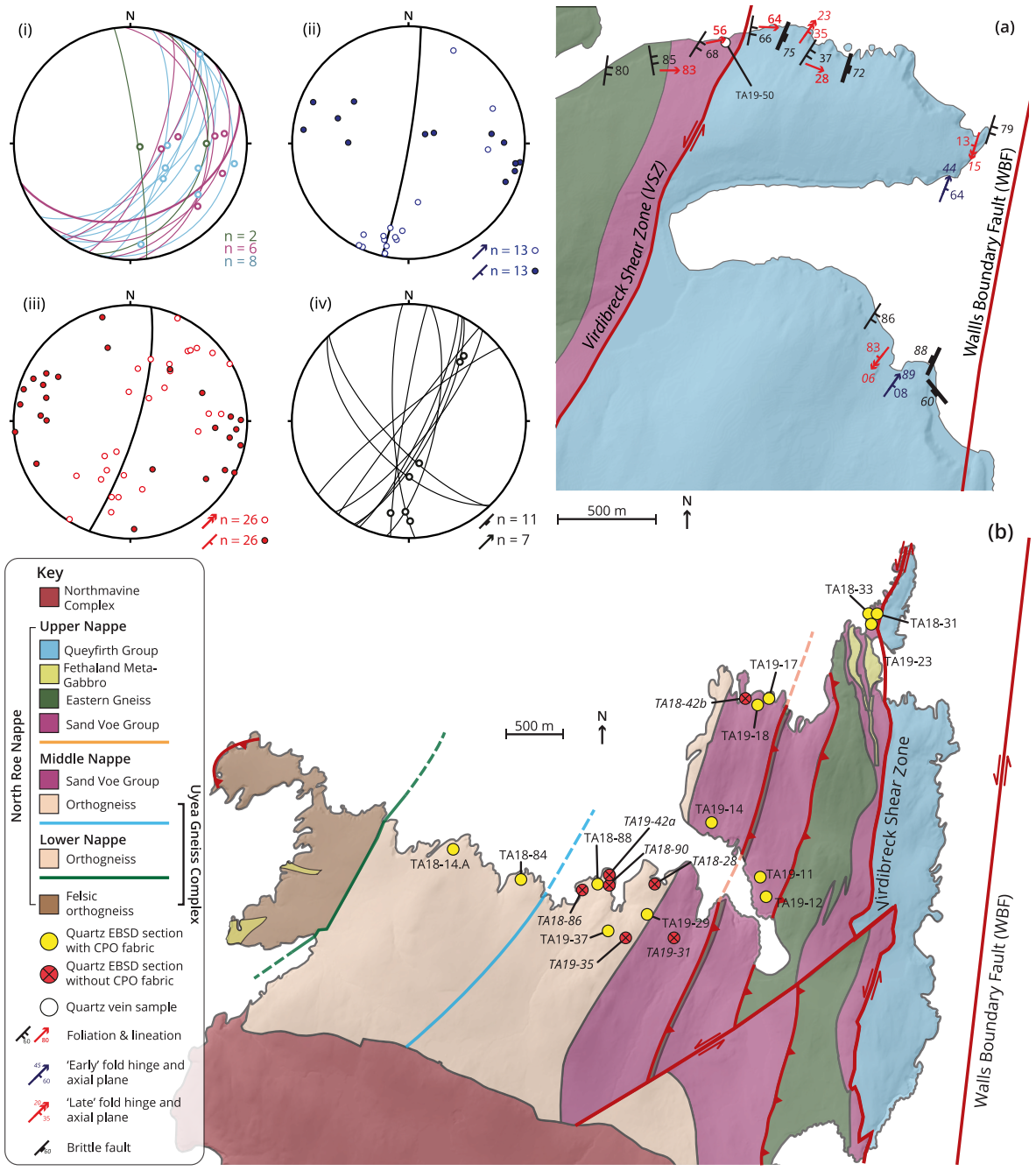

Fig. 13. (**a**) Geological map for part of the Queyfirth peninsula showing foliation, lineation, folding and faults. Stereonets show: i) foliation and lineation measurements colour coordinated for their geological units; ii) 'Early' fold hinges and axial planes; iii) 'Late' fold hinges and axial planes; iv) brittle faults and slickenlines. (**b**) Geological map of NW Mainland Shetland, showing the locations of the EBSD samples.

4.1. Uyea gneiss complex

The primary mineralogy of the UGC granitic and mafic components comprises calcic and antiperthitic plagioclase feldspar + quartz + muscovite ± biotite ± k-feldspar ± hornblende ± pyroxene ± uralite, with epidote + zoisite/clinozoisite + chlorite as retrogression products (Fig. 14a and b). The Neoarchaean foliation is defined by trails of muscovite and biotite grains and elongate aggregates of partially recrystallised quartz, which wrap lenticular porphyroclasts of plagioclase (Fig. 14b). Recrystallised quartz is medium to fine-grained (<0.5 mm) and forms monomineralic ribbons that display a shape preferred orientation (SPO) of sub-equigranular and sub-polygonal grains. Larger quartz grains (*c.* 0.6 mm) have an undulose extinction and are thought to be relict grains, indicating that overall, the intensity of quartz recrystallisation is low. Porphyroclastic feldspars (<1.2 mm) are rounded, show inclusions of retrograde zoisite/clinozoisite, brittle cataclasis, undulose extinction and mechanical kinking (Fig. 14b). Pyroxenes are usually only preserved as local relict grains wrapped by the quartz fabric and are partially to completely pseudomorphed by fine-grained intergrown uralitic amphibole (Fig. 14a). Hornblende grains are randomly aligned and are locally replaced by fine grained epidote and chlorite. Collectively, the mineral assemblages present suggest an amphibolite facies regional metamorphism for Neoarchaean deformation, overprinted by a static greenschist facies retrogression (see also Kinny et al., 2019).

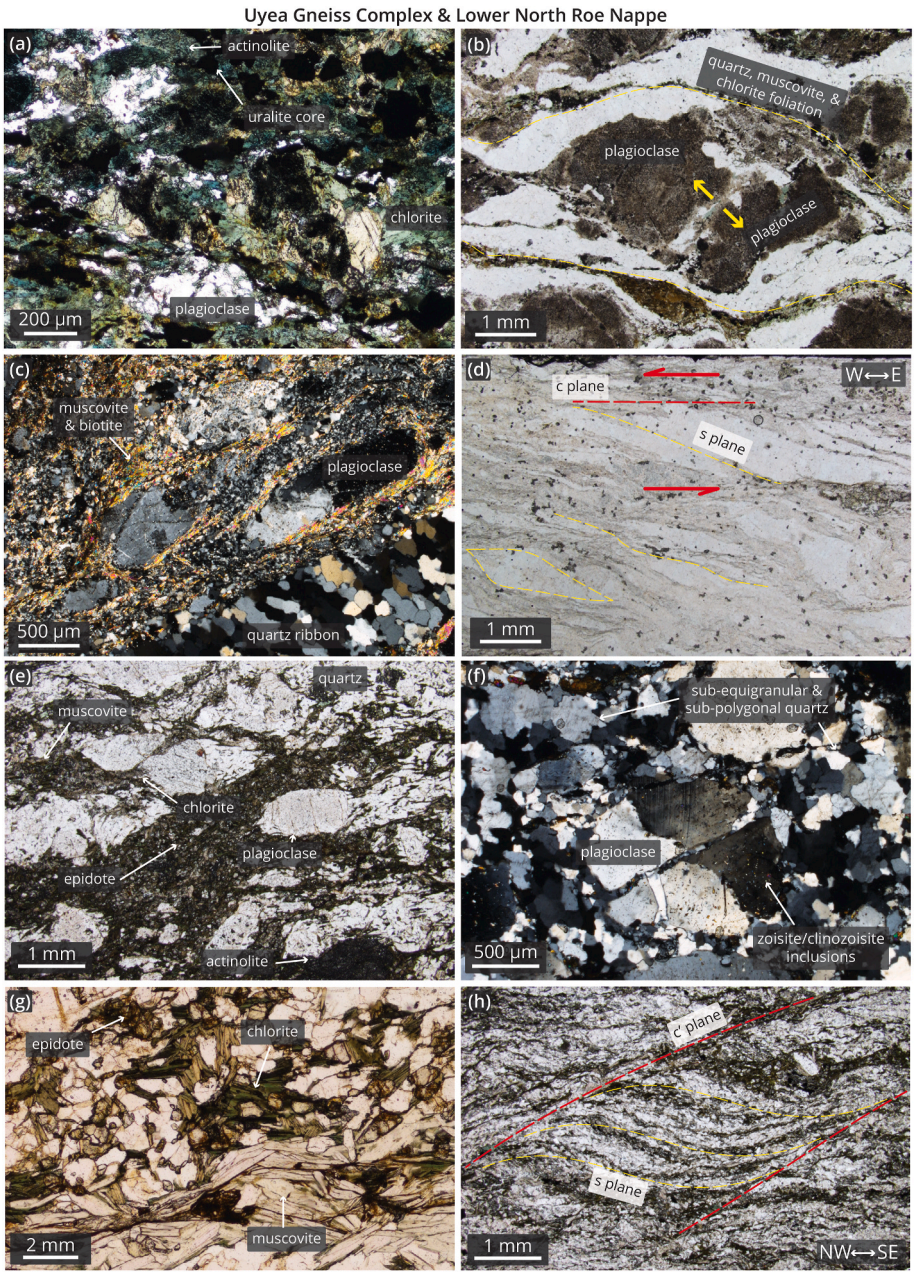

Fig. 14. Photomicrographs from the Uyea Gneiss Complex (a–d) and Lower NRN (e–h). (**a**) Amphibolitic metagabbro in the Uyea Gneiss Complex, showing uralisation of pyroxene to amphibole and chlorite (PPL) (HU 31993 92890). (**b**) Porphyroclastic plagioclase grains showing intense saussurisation and brittle cataclasis (PPL) (31433 91594). (**c**) Sample from a mylonite micro shear zone in the Uyea Gneiss Complex, showing fine-grained material and quartz ribbons flanked by fine-grained micas (XPL) (HU 31202 93178). (**d**) S-C fabric showing a top-to-the W shear sense in a mylonitic micro shear zone (PPL) (HU 31202 93178). (**e**) Representative orthogneissic composition, Lower NRN (PPL) (HU 33104 92159). (**f**) Equigranular quartz grains surrounding a porphyroclastic plagioclase grain. The plagioclase grain exhibits brittle cataclasis and kinking and deformation lamellae (XPL) (HU 32979 92173). (**g**) Greenschist facies mineral assemblage, including muscovite, chlorite and epidote (PPL) (HU 32979 92173). (**h**) S-C shear fabric showing top-to-the-NW kinematic (PPL) (HU 33746, 91862).

Later shear zones comprising finer grained proto- to ultramylonites show a foliation defined by an alignment of biotite, muscovite and interbanding of quartz and feldspar rich horizons (Fig. 14c). Quartz grains display pervasive recrystallisation and appear as elongate ribbons with polygonal, equigranular textures and display a weak SPO likely due to SGR dynamic recrystallisation (Fig. 14d). Finer grained (<0.1 mm) recrystallised quartz grains are preserved in polymineralic layers presumably reflecting the effects of Zenner pinning by distributed fine (0.2 mm) mica grains during grain growth (Fig. 14c; Vernon, 2004). Relict feldspar porphyroclasts show limited recrystallisation of fine-grained material (<50 μm) around grain boundaries (Fig. 14c). Feldspar clasts exhibit a sweeping undulose extinction with inclusions of sericite/clinozoisite and are locally brittlely deformed. Tight W-verging microfolds and asymmetric S-C fabrics suggest a top-to-the W shear (Fig. 14d). Collectively, these features suggest a lower- to mid-greenschist facies (300–400 °C) temperature for mylonite development, possibly contemporaneous with the static greenschist retrogression seen outside the mylonite zones in areas dominated by older Neoarchaean deformation (e.g. Fig. 14a and b).

4.2. Lower North Roe Nappe orthogneisses

The orthogneisses forming the Lower NRN typically comprise plagioclase + quartz + muscovite ± biotite ± k feldspar + actinolite +

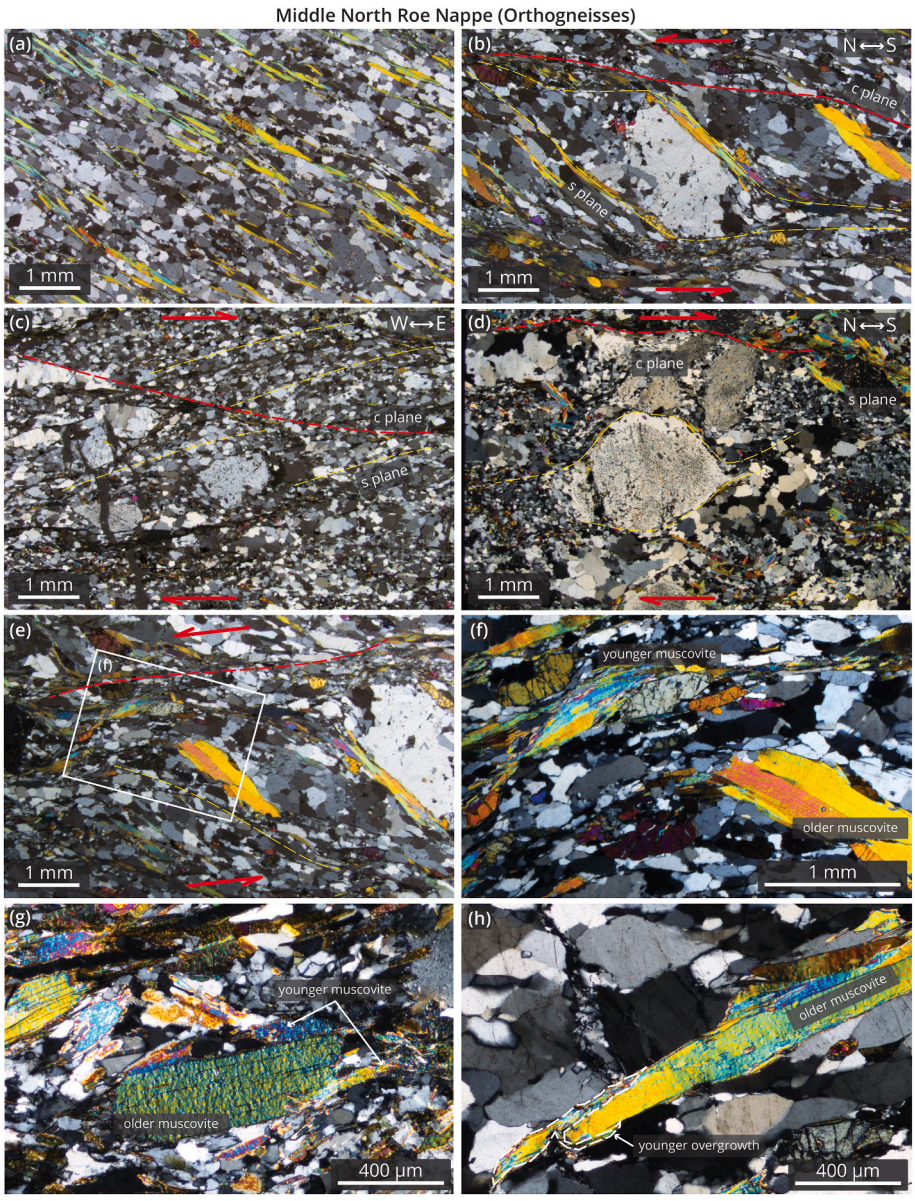

Fig. 15. Photomicrographs in XPL of the orthogneiss from the Middle North Roe Nappe. (**a**) Relatively highly strained, mylonitic foliation defined by LPO and CPO of quartz and muscovite, coaxially deformed domain (HU35403, 91473). (**b**) Sinistrally sheared asymmetric plagioclase porphyroclast and quartz aggregate pressure shadow, asymmetric transition from the Middle Nappe (HU 35196, 91246). (**c**) Top-to-the-E extensional S-C shear fabric, asymmetric transition from the Middle Nappe (HU35960, 93696). (**d**) Dextral shear sense and wrapped, internally fractured porphyroclastic plagioclase, asymmetric transition from the Middle Nappe (HU 434892 1191843). (**e**) Sinistral S-C shear fabric defined by fine grained and porphyroclastic muscovite generations (HU 35196, 91246). (**f**) insert photo from a, showing S-C shears cross cutting porphyroclastic muscovite (HU 35196, 91246). (**g**) Fibrous ('beardy') overgrowths and fine-grained muscovite overgrowing porphyroclastic muscovite (HU 35544, 91301). (**h**) Beardy overgrowth of fine-grained muscovite on porphyroclastic (Neoproterozoic?) muscovite (HU 435196 1191246).

epidote with a chlorite ± clinozoisite/zoisite retrograde assemblage (Fig. 14e–h). Quartzofeldspathic horizons have typically developed a protomylonitic foliation. Quartz grains are often pervasively recrystallised in monomineralic ribbons which show sub- to equigranular and sub- to polygonal grains (Fig. 14f). Quartz grains are medium sized (*c.* 0.5 mm) and show a strong SPO with a probable high degree of crystallographic preferred orientation highlighted by the uniformity in grain colours using a sensitive tint plate, consistent with dynamic SGR recrystallisation. Feldspars show a distinctive bimodal grain size population. Coarse grained porphyroclastic (0.8 mm) calcic plagioclase grains are partially recrystallised, and show rounded to sub-euhedral textures, undulose extinction, kinking, cataclasis, core and mantle structures and fine zoisite/clinozoisite inclusions (Fig. 14f). These are surrounded by smaller feldspar grains (0.1–0.3 mm) which display a localized SPO. This suggests a combination of brittle cataclasis, bulging recrystallisation (BLG) and/or pressure solution for feldspar deformation. Actinolite is pervasively replaced by chlorite whilst muscovite is medium to fine grained and is intergrown with likely co-genetic epidote (Fig. 14g). Almost all examples of asymmetric pressure shadows, shear fabrics and verging folds suggest top-to-the-NW shear sense consistent with field observations (Fig. 14h). Based on the quartz – feldspar deformation textures and mineral assemblages, deformation associated with the main fabrics preserved in these rocks is thought to have occurred at mid-upper greenschist facies conditions (ca. 400–500 °C; Stipp et al., 2002).

Quartz vein EBSD samples TA1814 and TA1884 were collected from

Fig. 16. Photomicrographs of the microstructural features of the Sand Voe Group. (**a**) Monomineralic quartz ribbons showing serrate and interlobate textures, flanked by muscovite grains) (XPL) (HU 35549 91301). (**b**) Quartz textures showing serrate and concave grain boundaries in quartz rich domains (centre) vs finer grained regions of equigranular, polygonal quartz in polymineralic layers reflecting grain boundary pinning (XPL) (HU 36352 93532). (**c**) Internal subgrain development in quartz (HU 36352 93532) (XPL). (**d**) Porphyroclastic plagioclase displaying core and mantle texture and undulose extinction (XPL) (HU 35892 92347). (**e**) Rotated pre-/syn- tectonic garnet wrapped by biotite, muscovite and chlorite and sinistrally sheared (PPL) (HU 35549 91301). (**f**) Close to the orthogneiss-Sand Voe Group contact, rare porphyroclastic grains of muscovite (>1 mm) are overgrown by finer (0.1–0.2 mm) colourless/brown muscovites, suggesting two generations of mica growth (XPL) (HU 35892 92347).

areas in the Lower NRN that showed down-dip mineral lineations and top-to-the-NW shear sense (Fig. 14). The former exhibits both elongate and porphyroclastic (>1 mm) quartz grains (Fig. 19a). The former represents the main recrystallisation fabric and has an average recrystallised grain size of 91.4 ± 63.1 mm, indicative of a differential stress of 26 MPa. However, both contribute to a clustered c-axis fabric subnormal to foliation, suggesting top-to-the NW shear. Such a fabric is indicative of basal <a> crystal slip consistent with BLG and SGR dynamic recrystallisation and hence greenschist facies conditions (Schmid and Casey 1986; Stipp et al., 2002). In contrast, sample TA1884 comprises dominantly relict porphyroclastic grains (0.8–1.2 mm) with a uniform texture (Fig. 19b). Its c-axis pole figure comprises several clusters that are related to individual grain orientations and hence cannot be used to constrain deformation kinematics, although detailed analysis of dispersion patterns revealed by individual clusters may indicate specific crystal slip systems. The recrystallised fraction has a mean grain size of 146.0 ± 97.0 mm, indicating a potential differential stress of 20 MPa.

Based on the quartz – feldspar deformation textures and mineral assemblages, deformation associated with the main fabrics preserved in the Lower NRN is thought to have occurred at mid-upper greenschist facies conditions (ca. 400–500 °C; Stipp et al., 2002) (Fig. 20). Differential stresses from mean recrystallised grain sizes indicate strain-rates of ~5 × 10^{-13} to somewhat faster than 10^{-12} s^{-1} (Lusk et al., 2021).

4.3. Middle North Roe Nappe orthogneisses

Deformed orthogneisses from the Middle NRN are mineralogically similar to those in the Lower NRN (Fig. 15a–d). However, the proportion of dynamically recrystallised quartz grains is higher and the grain size is overall lower in the Middle NRN, consistent with the field observation that the strain increases up-section and to the east. In samples from asymmetric transitions, medium sized (c. 0.4 mm) quartz grains are pervasively recrystallised as equigranular and polygonal grains with a very consistent mineralogical alignment and well developed SPO, forming an intense foliation (e.g. Fig. 15b–c). The majority of quartz grains are therefore thought to be recrystallised via SGR, although minor amounts of GBM and grain boundary area reduction/static recrystallisation have occurred. In samples from symmetric transitions, coarse- to

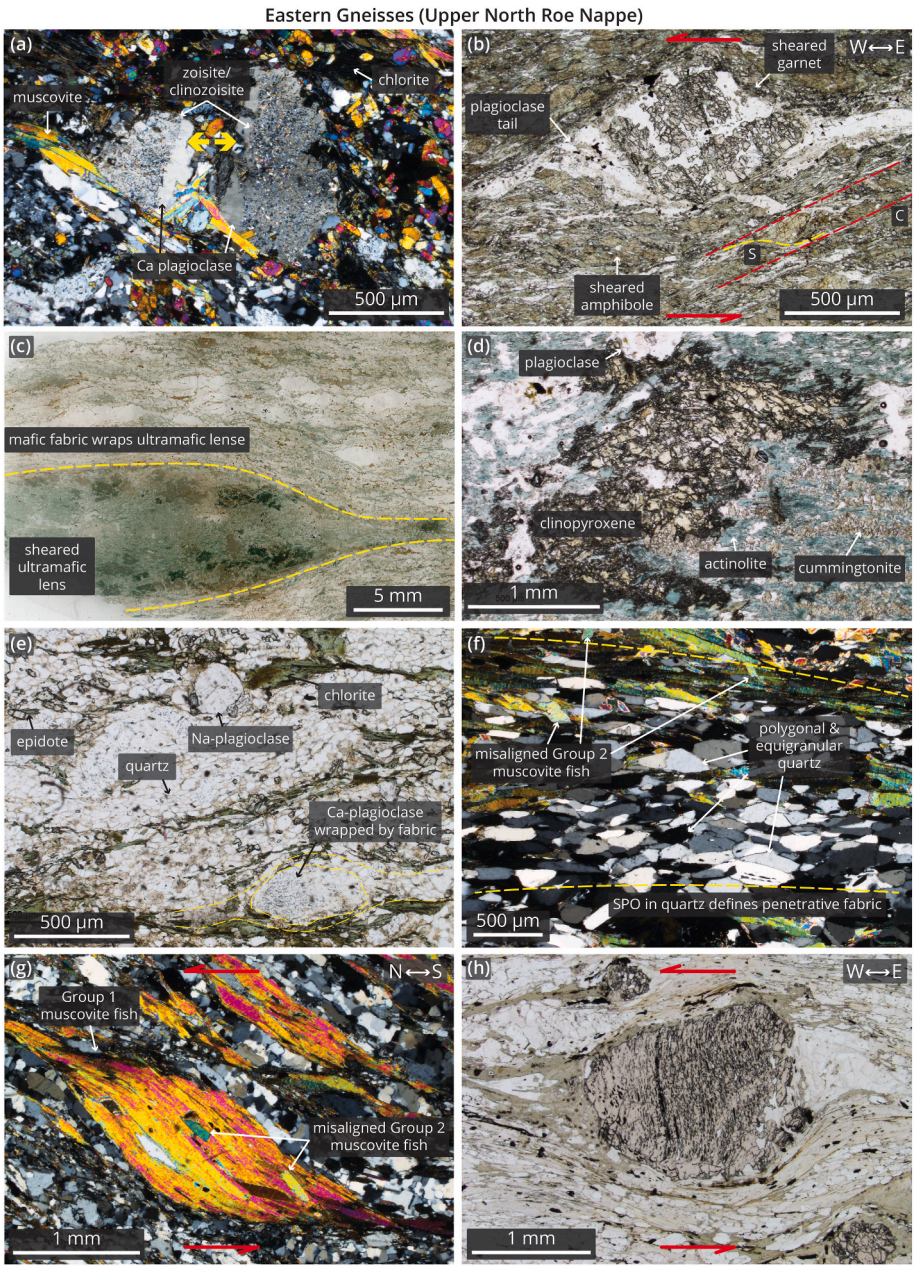

Fig. 17. Photomicrographs of the microstructural features for ultramafic and mafic components of the Eastern Gneiss. (**a**) Porphyroclastic plagioclase with retrograde zoisite/clinozoisite inclusions. Plagioclase shows brittle cataclasis (XPL) (HU 37032 93414) (**b**) Sheared amphibolite showing SPO orientated forming the S foliation of an S-C fabric. Garnet is sheared and wrapped by a tail of plagioclase. Garnet tail and S-C fabric show a top-to-the W shear sense (PPL) (HU 38239 94288). (**c**) Ultramafic lens of amphiboles (green) and pyroxenes (brown; PPL reflected light scan) surrounded by amphibolite (amphibole, plagioclase, biotite, secondary chlorite, quartz) (HU 37142 92818). (**d**) Clinopyroxene regressed to actinolite and cummingtonite amphiboles in uralisation in an ultramafic lens (PPL) (HU 37142 92818). (**e**) Composition and general structure of felsic Eastern Gneiss (PPL) (HU 37032 93414). (**f**) Polygonal, equigranular, sheared quartz grains with a strong SPO, (Bennigarth Pelite (XPL) (HU 35901 83008). (**g**) Muscovite fish showing a top-to-the W shear sense, Bennigarth Pelite (XPL) (HU 37181 93967). (**h**) Pre/syn-tectonic garnet with a rotated internal inclusion fabric. Wrapping the garnet is a quartz-muscovite fabric showing very open flanking folds and top-to-the W shear sense (PPL) (HU 35901 83008).

medium-sized quartz grains (*c.* 0.7 mm) show long straight grain boundaries and polygonal textures, suggesting that the dominant deformation mechanisms were associated with extensive syn-kinematic grain boundary reduction (e.g. Fig. 15a). Medium grained (*c.* 0.4 mm) calcic plagioclase feldspars are partially recrystallised and show undulose extinction, kinking, cataclasis, core and mantle structures and minor zoisite/clinozoisite inclusions (Fig. 15b–d). Porphyroclastic feldspars have strain shadows and 'beard-like' overgrowths of fine-grained plagioclase, muscovite, biotite and chlorite (Fig. 15b–d).

Porphyroclastic (0.6–1 mm) muscovite and more common, finer grained (<0.25 mm) muscovite grains are interpreted to represent two different generations of mica (Fig. 15e–h). Where present together, porphyroclastic grains show 'beard-like' overgrowths of fine-grained muscovite. Texturally similar fine muscovites also occur in shear bands, suggesting a coeval age for the smaller grains and S-C fabric formation. Thrust, extensional, sinistral and dextrally deformed horizons are all associated with texturally identical S-C fabrics and asymmetrically sheared porphyroclasts. No evidence is present which suggests overprinting or reworking of fabrics with differing shear senses. Therefore, the varying kinematic shearing events are considered to be

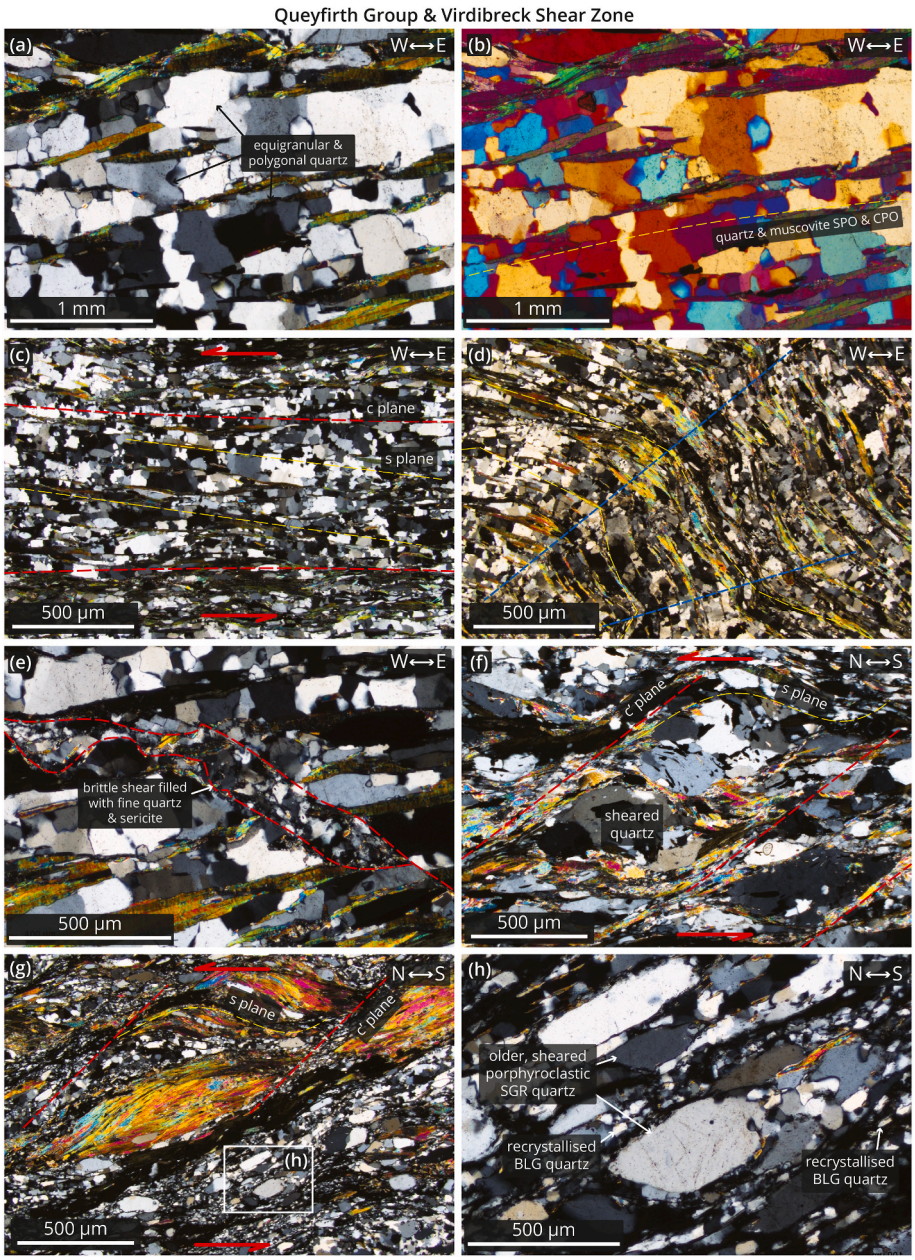

Fig. 18. Photomicrographs of the microstructural features for the Queyfirth Group and the VSZ (all XPL). (**a**) Recrystallised quartz textures and quartz ribbons in a psammite from the Queyfirth Group (HU 35934 83027). (**b**) Same view as (a) with sensitive tint plate. (**c**) Top-to-the W shears in the Queyfirth Group, Queyfirth Peninsular (HU 35934 83027). (**d**) 'Z' -shaped dextrally verging microfold (HU 35934 83027). (**e**) Brittle shear infilled with very fine-grained quartz, sericite and calcite (HU 35934 83027). (**f**) Sheared quartz aggregate wrapped by muscovite and fine-grained recrystallised quartz. Shows top-to-the N shear sense (HU 37503 94384). (**g**) Type 1–3 muscovite fish (sensu ten Grotenhuis et al., 2003) and highly sheared quartz denoting top-to-the N shear sense (HU 37633 93621). (**h**) Close up of (g), showing older SGR-recrystallised quartz grains wrapped by very fine grained BLG-recrystallised quartz material (HU 37633 93621).

broadly simultaneous on textural grounds. Based on the quartz and feldspar deformation textures and mineral assemblages, deformation is thought to have occurred under upper-greenschist to lower-amphibolite facies temperature (450–550 °C) conditions (Stipp et al., 2002) (Fig. 20).

Quartz vein samples TA1937 and TA1929 were collected from outcrops of the Middle NRN that show sinistral shear in the orthogneiss host rocks for EBSD analysis; the latter was within ~50 m of the contact with the Sand Voe Group (Fig. 13b). Both samples were cut in a section orientated N-S. They comprise relatively coarse relict porphyroclastic grains, with TA1937 having grains >1 mm with highly serrated and interlobate grain boundaries (Fig. 19c) and TA1929 having grains between 0.6 and 1 mm with grain boundaries that are in places serrated and in places polygonal (Fig. 19d). Recrystallised grains represent relatively minor fractions, with average grain sizes of 127 ± 91.9 mm (TA1937) and 162.0 ± 122.0 mm (TA1929), indicating differential stresses of 21 MPa and 18 MPa, respectively. The c-axis pole figures comprise clusters related to individual grain orientations (Fig. 19c and d) and hence cannot be used to constrain deformation kinematics, although further detailed analysis of dispersion patterns revealed by individual clusters may indicate specific crystal slip systems.

Based on the quartz and feldspar deformation textures and mineral assemblages, deformation is thought to have occurred under upper-greenschist to lower-amphibolite facies temperature (450–550 °C) conditions (Stipp et al., 2002) (Fig. 20). Differential stresses from mean recrystallised grain sizes indicate strain-rates somewhat slower to those for the lower NRN of ~3–6 x 10^{-13} s^{-1} (Lusk et al., 2021).

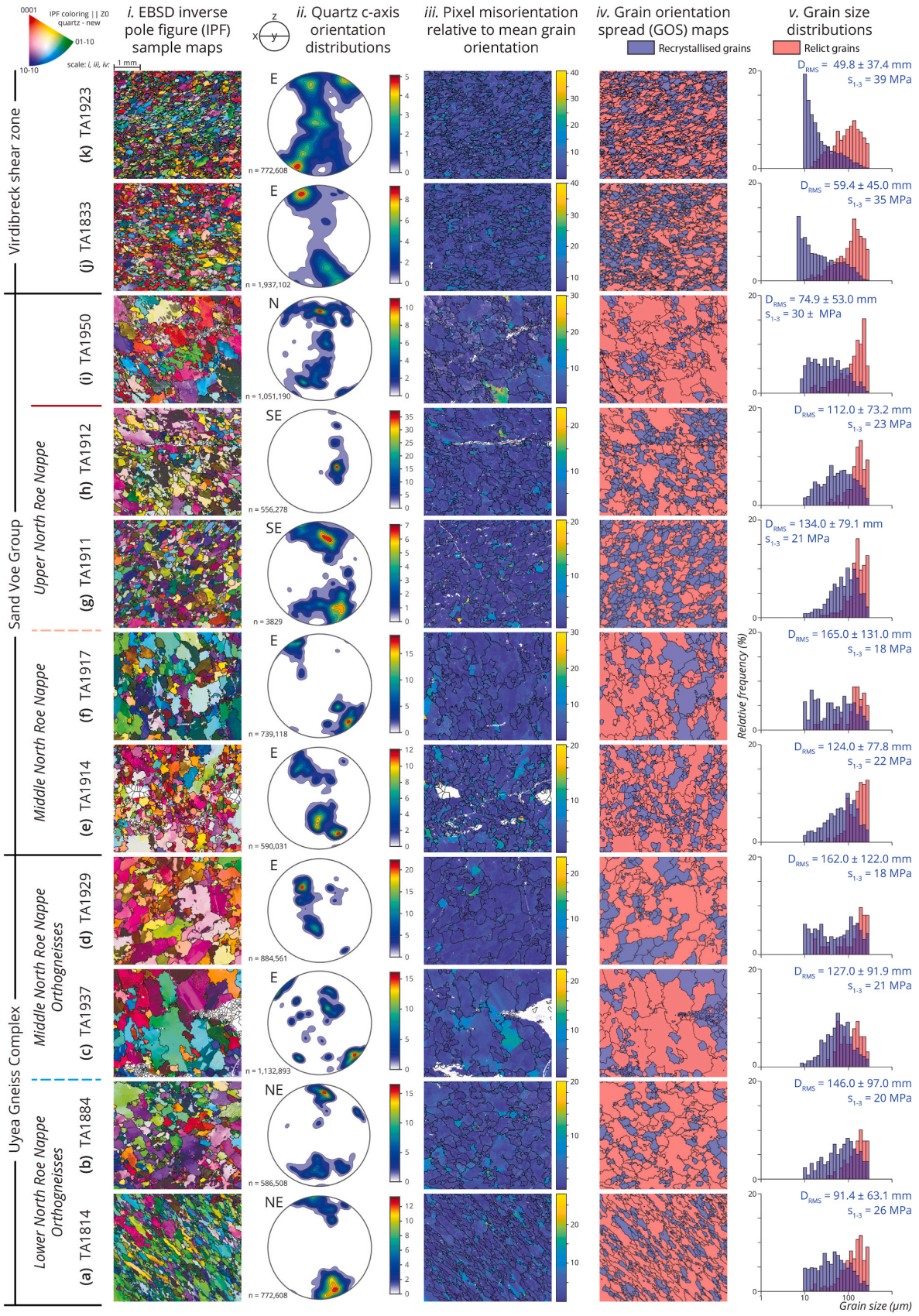

Fig. 19. a–k. Summary of EBSD (columns 1, 2) and dynamic recrystallisation grain size (columns 3, 5; Cross et al., 2017) analyses of quartz veins and segregations in the North Roe Nappe. See text for discussion.

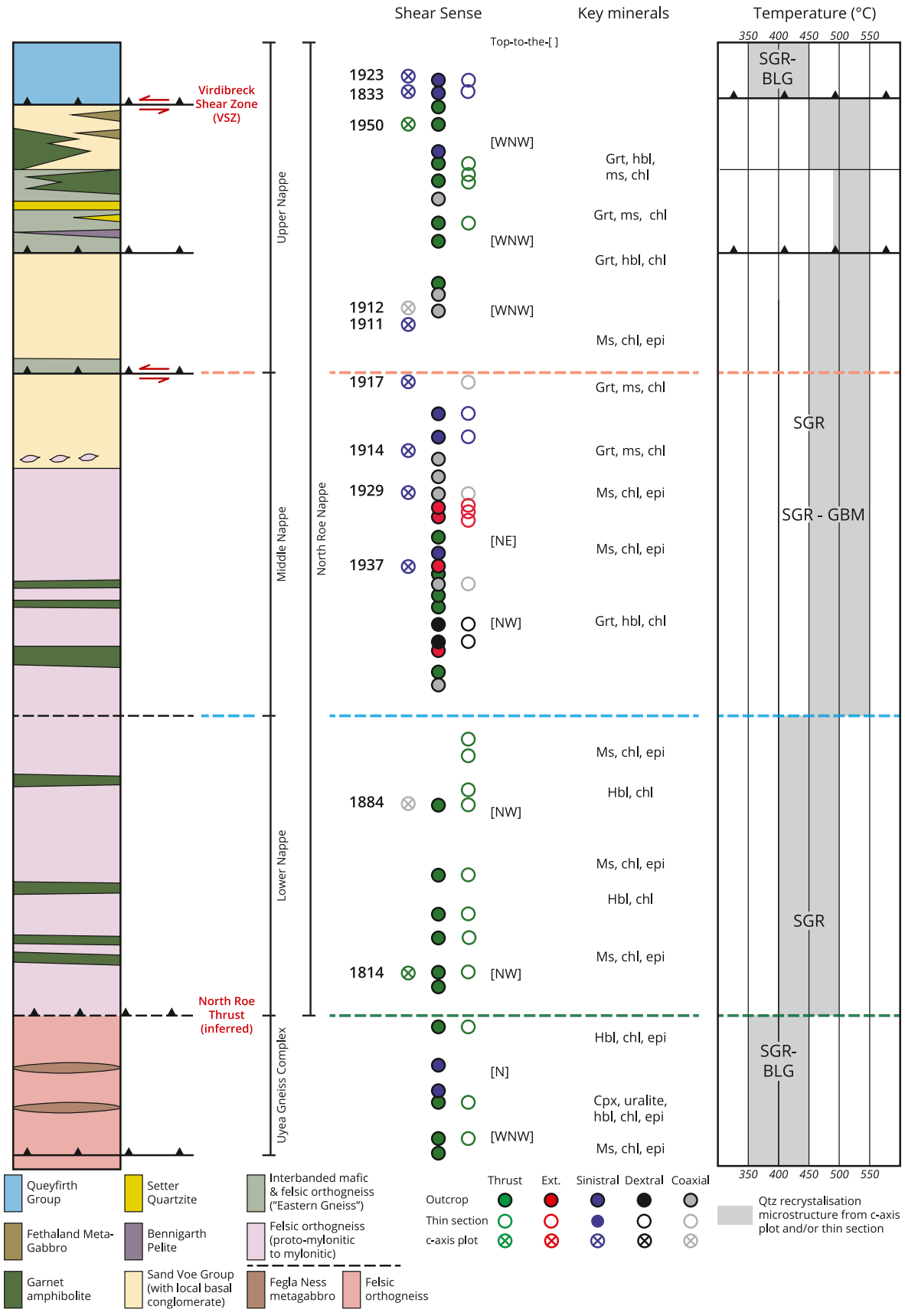

Fig. 20. Tectonostratigraphic column, with (from L to R): field shear sense orientations; optical and c-axes data sets; key minerals present; microstructural temperature estimates.

4.4. Sand Voe group

The Sand Voe Group is typically composed of quartz + plagioclase + muscovite ± biotite ± epidote ± chlorite ± garnet (Fig. 16a–f). Quartz is almost completely recrystallised as strain-free equigranular and polygonal grains (0.4–0.6 mm) that define the main foliation in monomineralic ribbons (Fig. 16a–c). In more polymineralic areas, quartz grains may show serrated and concave grain boundaries (Fig. 16b), or internal subgrains (e.g. Fig. 16c). Quartz grains may also be pinned by muscovite leading to marked differences in grainsize between polymineralic layers and monomineralic ribbons (Fig. 16a–c). Collectively the observations indicate that a combination of SGR and GBM recrystallisation mechanisms were active. Porphyroclastic plagioclase grains are in places partly recrystallised and display core and mantle textures and undulose extinction (Fig. 16d). Garnets (>1 mm) are wrapped by the foliation, show no internal inclusion trails and are considered to be pre- or syn-deformational porphyroblasts (Fig. 16e). Commonly, feldspar grains and garnets show asymmetric pressure shadows infilled with epidote, muscovite and biotite. Muscovite grains form either as colourless or slightly pleochroic pale-brown colours and are medium- to fine-grained (0.6–0.2 mm). Muscovites are mostly acicular and equigranular with a strong SPO and alignment of basal planes. Notably, in samples closer to the lower orthogneiss-Sand Voe Group contact, porphyroclastic muscovites occur (>0.8 mm) showing either thick and stumpy shapes with cleavage oblique to foliation, or elongate and tabular shapes parallel to foliation with a sweeping undulose extinction. Thin fine overgrowths (<0.1 mm), comprising feldspar, muscovite, biotite and chlorite, are identified on the porphyroclasts which again suggests two generations of mica growth (Fig. 16f). Quartz and feldspar deformation textures are consistent with upper-greenschist/lower-amphibolite facies temperatures (450–550 °C; Stipp et al., 2002) (Fig. 20). Asymmetric pressure shadows infilled with a greenschist facies assemblage of fine-grained muscovite and chlorite, rotated garnets and S-C fabrics indicate that N-S sinistral shear occurred during greenschist facies deformation (Fig. 16e), i.e., the younger retrograde minerals – including fine muscovite - formed during sinistral deformation.

Five quartz veins (TA1914, TA1917, TA1911, TA1912, TA1950; see Fig. 14 for locations) were sampled from the Sand Voe Group for EBSD analysis. Samples TA1914 and TA1917 were collected from within *c.* 100 m of the orthogneiss-Sand Voe Group contact and from areas showing a shallow NE-plunging or horizontal N-S trending mineral lineation. Samples TA1911 and TA1912 were collected from the Upper NRN exhibiting a NE-trending lineation in outcrop. Sample TA1950 was collected from the Queyfirth Peninsular (Fig. 13a) with an east plunging mineral lineation in outcrop. The samples exhibit distinct variations in grain size both across the Sand Voe Group as a whole and within/between the different nappe units (Fig. 19e–i). The lowermost samples (TA1914 and TA1917) exhibit relict grain sizes of between 0.6 and 1 mm. TA1914 exhibits polygonal grain boundaries, whilst larger porphyroblastic grains have internal subgrains (Fig. 19e). TA1917 has a mixture of polygonal and serrate-interlobate grain boundaries, with larger grains again showing internal subgrains (Fig. 19f). The recrystallised fractions have mean grain sizes of 124.0 ± 77.8 mm (TA1914) and 165.0 ± 131.0 mm (TA1917), indicating differential stresses of 22 MPa and 18 MPa respectively. The middle Sand Voe Group samples (TA1911 and TA1912) comprise respectively equigranular ~0.6 mm and 0.3–0.6 mm sized grains with straight polygonal boundaries (Fig. 19g and h) and rare ~1 mm grains slightly misaligned to the main fabric and internal subgrains. TA1911 has a somewhat greater recrystallised grain fraction than TA1912 (Fig. 19g), with a mean grain size of 134.0 ± 79.1 mm compared to 112.0 ± 73.2 mm (Fig. 19h), indicating differential stresses of 21 MPa and 23 MPa respectively. The uppermost sample (TA1950) exhibits a range of relict grain sizes from 0.3 to >1 mm (Fig. 19i). Grain textures show a mixture of polygonal and serrate-interlobate grain boundaries, with larger grains showing internal subgrains consistent with greenschist facies conditions. The recrystallised fraction has a mean grain size of 74.9 ± 53.0 mm, indicating a differential stress of 30 MPa.

In general, the five quartz veins sampled from the Sand Voe Group exhibit ambiguous c-axis fabrics (Fig. 19e–i) unsuitable for characterisation of deformation type and/or 'opening angle' thermometry (e.g. Faleiros et al., 2016). Most reflect the relatively large relict grain sizes present in the samples and hence represent orientation clusters derived from individual grains. At best, they are suggestive of single girdles and lack well-defined cross-girdle fabrics (indicating approximate plane strain deformation) or small circle girdle distributions centred about the pole to foliation (indicating deformation in the flattening field), although TA1950 has a hint of a small circle distribution centred about the pole to foliation that perhaps indicates flattening deformation. Indeed, it is possible arguably to estimate an opening angle of 67° and hence a deformation temperature of 515 °C via the Faleiros et al. (2016) linear opening angle thermometer; however, this temperature does seem rather high compared with other evidence presented.

Quartz and feldspar deformation textures are consistent with upper-greenschist/lower-amphibolite facies temperatures (450–550 °C; Stipp et al., 2002) (Fig. 20). Asymmetric pressure shadows infilled with a greenschist facies assemblage of fine-grained muscovite and chlorite, rotated garnets and S-C fabrics indicate that N-S sinistral shear occurred during greenschist facies deformation (Fig. 16e), i.e., the younger retrograde minerals – including fine muscovite – formed during sinistral deformation. Differential stresses from mean recrystallised grain sizes indicate a range of strain-rates depending on whether the quartz veins responded to the higher or lower metamorphic conditions. However, in both cases, strain-rates increase from the lower, through the middle, to the upper NRN. For higher temperature cases, rates vary from somewhat slower than 10^{-12} s^{-1}, through ~10^{-12} s^{-1}, to ~5×10^{-12} s^{-1}, whilst for lower temperature cases, rates vary from ~3×10^{-14} s^{-1}, through ~10^{-13} s^{-1}, to ~2×10^{-13} s^{-1} (Lusk et al., 2021).

4.5. Eastern gneisses

Mafic components of the Eastern Gneiss typically comprise Na- and Ca-rich plagioclase + cummingtonite + actinolite ± biotite ± epidote ± chlorite ± quartz ± garnet (Fig. 17a and b). Plagioclase grains are typically very fine grained (<0.2 mm) recrystalised aggregates with no SPO, although the grains show an alignment of fast or slow directions (extinction) when viewed using a gypsum sensitive tint plate. Larger porphyroclastic plagioclase grains (>0.6 mm) typically show saussuritization, brittle cataclasis, sweeping undulose extinction and are wrapped by a mineralogical foliation defined by fine-grained plagioclase (Fig. 17a). The characteristics displayed by plagioclase are indicative of BLG recrystallisation in fine-grained material, whilst brittle/viscous deformation mechanisms were active in porphyroclastic grains. Minor amounts of quartz are recrystallised as fine to medium (0.3–0.6 mm) grains with a weak SPO. Actinolite and cummingtonite also display undulose extinction, a pervasive mineral alignment, and appear as elongate grains aligned parallel to the foliation (Fig. 17b). Garnet porphyoblasts are coarse (>1 mm) and show inclusions of randomly non-aligned cummingtonite and plagioclase. However, garnets are wrapped by plagioclase and amphiboles indicating pre- or syn-tectonic growth (Fig. 17b). Ultramafic lenses of Eastern Gneiss occur as mm-scale lenses of amphibole and clinopyroxene wrapped by a highly aligned fabric of mafic grains (Fig. 17c). Clinopyroxenes are highly retrogressed and overgrown by actinolite during uralitisation (Fig. 17d). Chlorite and plagioclase are observed in asymmetric pressure shadows of garnets which along with S-C' fabrics, denote a top-to-the W/NW sense of shear in mafic components (Fig. 17b).

Felsic meta-igneous components of the Eastern Gneiss are composed of quartz, Na- and Ca-rich plagioclase, orthoclase, muscovite, epidote, garnet and chlorite (Fig. 17e). Quartz grains are completely recrystallised into medium sized (0.6 mm) polygonal and equigranular shapes, suggesting a dominant SGR deformation mechanism. Quartz grains have

a strong SPO, which along with aligned grains of muscovite and epidote, form a well-defined, penetrative fabric (Fig. 17f). Plagioclase is porphyroclastic, shows rounded grain edges and inclusions of zoisite/clinozoisite/muscovite due to saussurisation (Fig. 17e). Feldspars are not recrystallised, show no internal fabric and are wrapped by a fine grained (<0.2 mm) polymineralic fabric.

The Bennigarth Pelite is a garnet-mica schist. It shows similar quartz deformation characteristics to felsic meta-igneous components of the Eastern Gneiss (Fig. 17g and h). Muscovite grains are medium to coarse grained (0.6–0.8 mm) and display cleavage parallel to foliation, indicating they are group 1 and group 2 muscovite fish (*sensu* ten Grotenhuis et al., 2003) (Fig. 17g). Garnets are coarse (>1 mm) and display an internal slightly sigmoidal fabric of plagioclase and quartz inclusions, indicating that the garnet growth was pre- or syn-tectonic (Fig. 17h). Fine grained (<0.2 mm) quartz and muscovite display a strong orientation parallel to the main fabric and also occur in asymmetric pressure shadows wrapping garnets; these indicate top-to-the-W shear.

The Setter Quartzite is a medium grained rock containing quartz and minor Na-rich feldspar. Overgrowing quartz grains are very fine grained (<0.1 mm) calcite and sericite. Very fine-grained quartz, calcite and brecciated clasts of fine-grained quartz aggregates form in late brittle shears that cross-cut the main ductile fabric.

Collectively, the mineral assemblage and quartz-feldspar deformation textures present in the Eastern Gneiss, Bennigarth Pelite and Setter Quartzite indicate an upper-greenschist to lower-amphibolite facies deformation temperature of 490–550 °C during top-to-the W shear (Stipp et al., 2002) (Fig. 20).

4.6. The Queyfirth group

Psammites and mica-schists from the Queyfirth Group comprise quartz, muscovite, chlorite and highly retrogressed garnet. Quartz grains are medium sized (0.6 mm) and display equigranular and polygonal textures (Fig. 18a–b). A moderate mineral alignment and SPO is shown in quartz, which along with aligned muscovite, forms a penetrative fabric (Fig. 18b). The widespread preservation of internal subgrains in quartz indicate that SGR was the dominant deformation mechanism. Recrystallised quartz grains also commonly show a sweeping undulose extinction, suggesting that grains may have been overprinted at a lower temperature, post-recrystallisation. In more polymineralic areas, quartz grains are pinned and show reduced grain size (0.4 mm) and may form quartz ribbons flanked by muscovite (Fig. 18a–c). Feldspar is uncommon. Muscovites are medium- to coarse grained (0.8 mm long), tabular and elongate and form a strong SPO (Fig. 18b). S-C shears, defined by ribbons of quartz and muscovite orientated oblique to the main fabric, indicate a top-to-the-W shear sense (Fig. 18c). Based on quartz textures, deformation temperature is estimated at mid-greenschist facies (450 °C) during top-to-the W shearing (Fig. 20). Overprinting this are dextrally verging 'Z' -shaped kink folds defined by folded quartz fabrics and low-temperature brittle shears infilled with very fine-grained quartz, chlorite and sericite (Fig. 18d–e).

The top-to-the-W, mid-greenschist facies fabrics are overprinted by dextrally verging 'Z' -shaped kink folds defined by folded quartz fabrics and low-temperature brittle shears infilled with very fine-grained quartz, chlorite and sericite (Fig. 18d–e).

4.7. Virdibreck shear zone

Mica schists from the VSZ on the Point of Fethaland show a bimodal population of quartz grains. Coarse to medium quartz grains show sweeping undulose extinction, rounded grain shapes and moderate SPO (Fig. 18f). Subgrains are widespread within the larger quartz grains indicating the operation of SGR recrystallisation. Wrapping these coarse grains are finer-grained (<0.2 mm), apparently strain free quartz layers, forming a core-mantle microstructure around relict porphyroclasts (Fig. 18g and h), suggesting a possibly later lower-temperature BLG recrystallisation deformation mechanism. Muscovite grains (<1 mm) are aligned with their basal planes sub-parallel to the main fabric and form Group 2 fish (Fig. 18g, sensu ten Grotenhuis et al., 2003). However, in places, larger porphyroclastic muscovite grains are orientated oblique to the fabric forming Group 4 fish. Chlorite commonly replaces garnet suggesting greenschist facies retrogression. The earlier SGR dominant deformation is estimated to have occurred under mid-greenschist facies (450 °C) conditions based on quartz dynamic recrystallisation textures (e.g. Stipp et al., 2002). The development of asymmetric muscovite fish and S-C' shears indicating a top-to-the N shear sense (Fig. 18f–g) in the VSZ, which is estimated to have occurred during a later phase of deformation under mid-lower greenschist facies (350–450 °C) conditions.

Two vein samples (TA1923, TA1833) were collected from mica schists above the VSZ on the Point of Fethaland (Fig. 13b) for EBSD analysis. Both have grain size ranges generally between 0.2 and 0.6 mm with straight and polygonal grain boundaries (Fig. 19j and k); TA1923 exhibits a zone of apparent dextral shear in the sample centre. Larger (*c.* 0.8 mm) porphyroclastic grains also occur, slightly misaligned relative to the main fabric, and exhibit subgrains suggesting they are strained relict grains (Fig. 19k). Recrystallised grains predominate in both samples (Fig. 19j and k), with average grain sizes of 49.8 ± 37.4 mm (TA1923) and 59.4 ± 45.0 mm (TA1833), indicating differential stresses of 39 MPa and 35 MPa respectively. These are the largest stresses indicated by EBSD analysis. The c-axis pole figure obtained from TA1833 can be interpreted as an asymmetrical (top-to-the left or NW) 'cross-girdle' (Fig. 19j). It is therefore the only EBSD sample from which it is possible to confidently estimate an opening angle and hence a temperature of deformation via the Faleiros et al. (2016) linear opening angle thermometer. The opening angle indicated is 55°, suggesting a temperature of 430 °C. However, the c-axis fabric suggests deformation in the general constrictional field using the fabric topology criteria of Schmid and Casey (1986). The c-axis pole figure obtained from TA1950 is much less well-defined (Fig. 19i).

The earlier SGR dominant deformation is estimated to have occurred under mid-greenschist facies (450 °C) conditions based on quartz dynamic recrystallisation textures (e.g. Stipp et al., 2002). The development of asymmetric muscovite fish and S-C' shears indicating a top-to-the N shear sense (Fig. 18f–g) in the VSZ, which is estimated to have occurred during a later phase of deformation under mid-lower greenschist facies (350–450 °C) conditions (Fig. 20). Differential stresses from mean recrystallised grain sizes indicate strain-rates somewhat faster than 10^{-12} s^{-1} (Lusk et al., 2021).

5. Discussion

5.1. The ages of deformation events in NW mainland Shetland

Geochronological studies suggest that the NW Mainland Shetland region was subject to multiple tectonic episodes between the Neoarchean and the Lower Palaeozoic (Fig. 1d and 21a; Walker et al., 2016, 2020; Kinny et al., 2019). Here we review the likely ages of these deformational and metamorphic events and highlight the main areas of uncertainty that could be resolved by future geochronological studies.

5.1.1. The Uyea Gneiss complex

The evidence that the UGC is dominated by Neoarchaean deformation fabrics and metamorphic assemblages has been summarised earlier (Fig. 1d; see Kinny et al., 2019). The narrow, cross-cutting proto- to ultramylonitic top-to-the-W shear zones that rework the UGC show similar greenschist facies mineral assemblages, quartz deformation microstructures, and shear sense to those exhibited by the dominant foliation within the overlying orthogneisses of the North Roe Nappe, and hence these structures are assumed to be of broadly the same age (Fig. 21a).

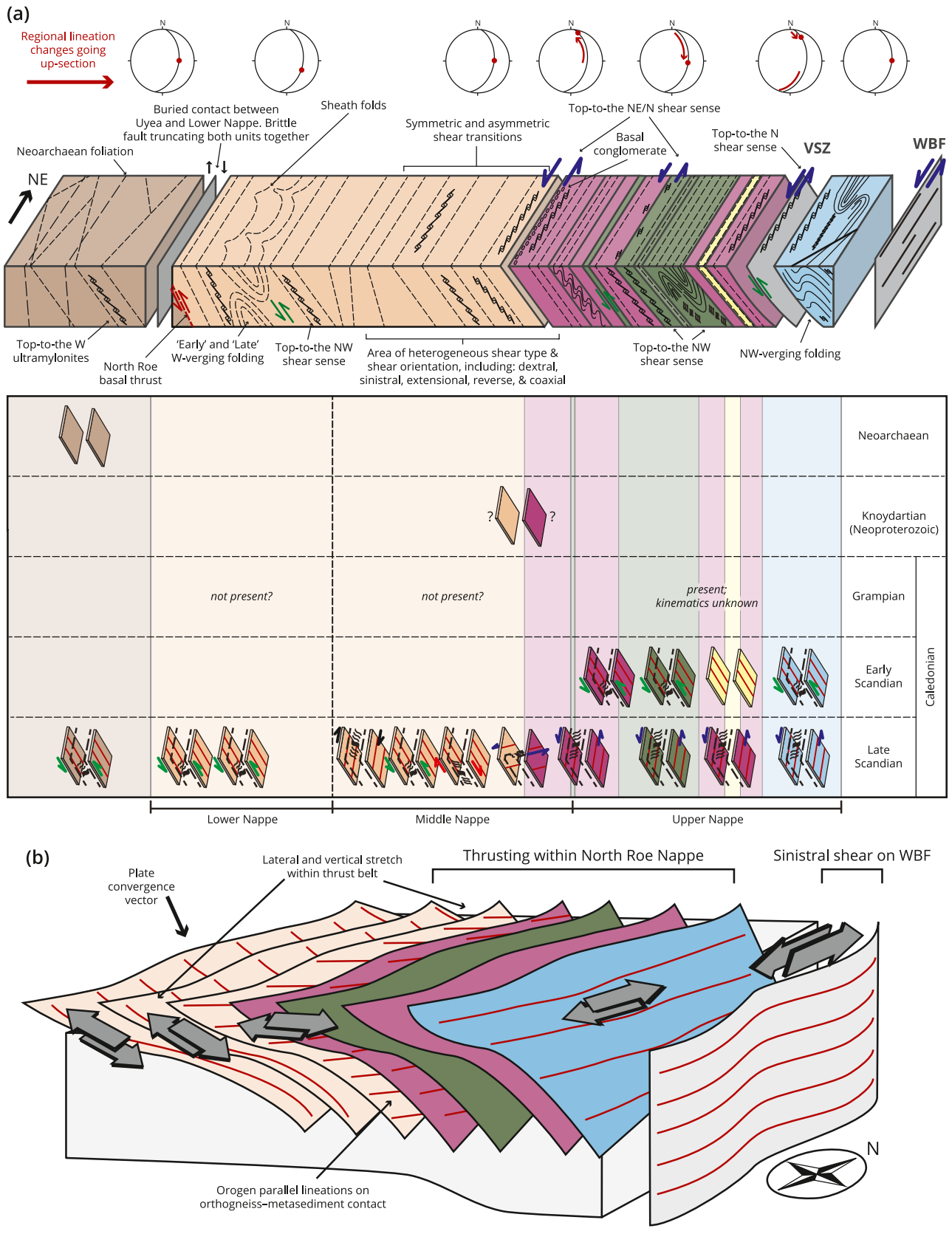

Fig. 21. (**a**) 3D block diagram (uppermost) and panel diagram (lowermost) for the North Roe Nappes summarising the kinematics and absolute ages of deformation. See text for further details. (**b**) Regional block diagram for the development of the North Roe Nappe under sinistral transpression. Dip-slip is concentrated at structurally lower levels of the Nappe, while the material close to the Walls Boundary Fault is sinistrally sheared.

5.1.2. Lower and Middle North Roe Nappes

Rb-Sr dating of muscovite grains that define the foliation in the Lower NRN has previously yielded ages of c. 411 and c. 416 Ma (Walker et al., 2016), and Lu-Hf dating of garnet from an amphibolite in the Middle North Roe Nappe gave an age of 427 ± 3 Ma (Fig. 1d). These results suggest that a significant element of metamorphism and deformation within the Lower and Middle North Roe nappes occurred during the Late Silurian to Earliest Devonian, corresponding to the later stages of the Scandian orogenic event (Walker et al., 2020).

However, structurally up-section to the east, above and below the orthogneiss-Sand Voe Group contact, Walker et al. (2016) obtained five Rb-Sr muscovite ages in the range 726–702 Ma which they interpreted as broadly dating deformation. These authors did not study the textural relationships of the dated muscovites in any detail. In contrast, the present study has recognised two generations of white mica growth at this level of the nappe pile. Older porphyroclastic grains orientated oblique to the main foliation are cross-cut by shears along which younger, fine grained micas are present; these younger shears are consistently the main kinematic indicators in all the structural domains documented above. We therefore suggest that the 726–702 Ma Rb-Sr ages obtained by Walker et al. (2016) may result from the mixing of older (800–750 Ma?; earlier, porphyroclastic) and younger (Caledonian; finer, later) mica populations, with the latter defining the main (Scandian) foliation as recognised at structurally lower levels in the nappe (Fig. 21a). Isotopic dating of the two mica populations is required to resolve the matter conclusively.

5.1.3. The upper North Roe nappe

Five Lu-Hf garnet ages have been published from the Upper North Roe Nappe (Fig. 1d; Walker et al., 2020). The three oldest were obtained from amphibolites. Two samples of Eastern Gneiss amphibolites yielded ages of 479.6 ± 1.2 Ma and 466.3 ± 2.2 Ma (Fig. 1d), and a Queyfirth amphibolite c. 6 km further south produced an age of 474.1 ± 3.8 Ma. Pelite horizons yield typically younger garnet ages as shown by the ages of 456.7 ± 2.2 Ma and 446.5 ± 1.3 Ma obtained from a Sand Voe Group pelite and the Bennigarth Pelite, respectively (Fig. 1d). The older group represents important evidence that the effects of the Grampian orogenic event extended west of the WBF. Importantly, however, the garnets within the Eastern Gneiss are porphyroclastic and are strongly wrapped by the main east-dipping foliation (e.g. Fig. 17b); there is no preserved evidence of older Grampian-aged fabrics (Fig. 21a). The younger group of garnet ages is plausibly related to the early stages of the Scandian orogenic event. These garnets are also wrapped by, and are hence older than the main foliation, but show sigmoidal inclusion trails suggesting syn-tectonic growth (e.g. Figs. 11d and 17h). An Rb-Sr muscovite age of 443.2 ± 1.3 Ma was obtained from a Sand Voe Group pelite close to the Virdibreck shear zone (Fig. 1d) and was interpreted to closely date foliation development (Walker et al., 2016). The working hypothesis adopted here is that the main east-dipping foliation formed during the Scandian orogenic event from c. 450 Ma onwards (Fig. 21a). Further detailed work is needed to establish the western limit of the effects of the Grampian orogenic event, and whether domains of older Caledonian and/or Knoydartian structures are preserved in areas of lower Scandian strain.

The main top-to-the W deformation fabrics in the Uppermost North Roe Nappe are cut by lower temperature, top-to-the N shears, including the Virdibreck Shear Zone (Fig. 21a). These are associated with a younger generation of finer grained muscovite and are kinematically compatible with the sinistral shearing observed at structurally lower levels. If the main foliations in the North Roe Nappe are Scandian in age, it follows that these younger top-to-the-N shears probably formed at a late stage in that orogenic event, but further detailed isotopic dating is required to confirm this hypothesis.

Low temperature, brittle, 'Z'-shaped dextral kinked folds and brittle faults rework the Queyfirth Group fabric on the Queyfirth Peninsular and brittle shears infilled with calcite are observed in the Eastern Gneiss. Similar dextral 'Z'-shaped folds and brittle shears were observed in both the field and thin sections from the Queyfirth Group at Ollaberry by Armitage et al. (2021) and were ascribed by these authors to the dextral reactivation of the WBF during the Late Carboniferous.

5.2. The western limit of Caledonian thrusting in the NW Mainland

Due to its stratigraphic location and highly strained nature, the contact between the orthogneiss and overlying Sand Voe Group (the Wester Keolka Shear Zone of Pringle, 1970) had been interpreted previously as a discrete tectonic break dividing regions dominated by Caledonian deformation (to the east) and pre-Caledonian deformation (to the west). This led to this shear zone being referred to as the northern continuation of the Moine Thrust (e.g. Andrews 1985; Ritchie et al., 1987; Flinn 1992, 1993). However, this contact may in fact be a deformed basement-cover unconformity (Pringle 1970; Walker et al., 2016), and it is also clear that the limit of pervasive top-to-the-NW ductile thrusting lies some 5 km further to the west (Figs. 1d and 2). We suggest that the North Roe Nappe is underlain by a basal thrust, the North Roe Thrust (Fig. 21a), which represents the western limit of ductile thrusting onshore and is a more plausible correlative of the Moine Thrust. Unfortunately, the boundary between the North Roe Nappe and the footwall Uyea Gneiss Complex is obscured by a later, presumably post-Caledonian brittle fault (Figs. 1d, 5b and 21a). It is also possible that the Uyea Gneiss Complex is itself also underlain by structurally lower Caledonian thrusts now located offshore.

5.3. Scandian transpressional tectonics

The oblique motions of tectonic plates at convergent margins commonly lead to transpressional deformation (Woodcock 1986; Fossen and Tikoff 1998; Teyssier and Tikoff 1998; Dewey et al., 1998; Lin et al., 1999; Jiang et al., 2001; Jones et al., 2004). In inclined shear zones like those seen in NW Shetland, transpression will in general lead to a bulk triaxial deformation which is non-coaxial and non-plane strain (e.g. Jiang et al., 2001; Jones et al., 2004, 2005). Natural transpressional (and transtensional) strains of this kind are commonly heterogeneously partitioned into domains of kinematically-related structures (e.g. Tavarnelli et al., 2004; de Paola et al., 2005; Jones et al., 2005). The strain patterns seen in one part of an individual shear zone may therefore not be representative of the bulk strain of the system (Jones et al., 2005).

The highly complex deformational partitioning seen across the North Roe Nappe shows many characteristics that can be interpreted as transpressional due to a combination of thrusting and sinistral strike slip (Fig. 21a and b). Across the Lower and Middle North Roe nappes, deformation appears on field and textural grounds to be coeval, but the distribution of strain (e.g. strain intensity, orientation, style, shear sense) is not evenly distributed. Most notably, there are horizons in the Middle NRN which show evidence for coeval dip-slip (thrust and extensional) and strike-slip (sinistral and dextral) deformation both on an outcrop and microstructural scale (Fig. 21b). In the Upper NRN, higher temperature top-to-the-west thrust-related fabrics are overprinted locally by lower temperature top-to-the N/NNE sinistral shearing. This suggests a complex structural evolution during the Scandian orogenic event, with a transition from early thrust-related deformation to younger sinistral strike-slip deformation which perhaps reflects the proximity of these rocks to the earliest phase of ductile displacement along the nearby Walls Boundary Fault (Fig. 21b; Watts et al., 2007, Armitage et al., 2021).

As there is no clear evidence to the contrary, we assume that the sinistral shearing seen at all levels in the NRN and top-to-the-NW dip-slip shear senses seen in the Lower & Middle North Roe nappes are the same age. The nappe system can be viewed therefore as an inclined domainal triclinic transpressive thrust system that partitioned strike-slip and dip-slip deformations into end member shear zones during at least the Scandian orogenic phase (Teyssier and Tikoff 1998; Jones et al.,

2004) (Fig. 21b). The NRN was presumably confined by the Walls Boundary Fault to the east, which likely acted as an important sinistral boundary condition (Fig. 21b). Dip-slip strain is therefore concentrated at structurally lower levels of the nappe, while strike-slip strain is most prevalent at structurally higher levels and closer to the Walls Boundary Fault.

The presence of top-to-the-SE extensional and NNE-SSW sinistral deformation in the Middle Nappe might be explained by a temporal progression from an early thrust-dominated shear zone, to a sinistrally-oblique extensional shear zone. In this model, later deformation would be focussed along the mechanically weaker orthogneiss-Sand Voe Group contact and into highly deformed parts of the Middle North Roe Nappe. This model, however, does not adequately explain how domains of antithetic NNE-SSW dextral shear sense and coaxially deformed horizons can also be present without overprinting relationships being present. It is therefore suggested that the presence of local domains of coeval syn- and antithetic deformation in a sinistrally transpressive thrust zone of this kind is better explained by invoking a localised differential strain rate within the shear zone (Jones et al., 1997) resulting in ductile vertical and lateral extrusion of coaxial domains along a series of foliation-parallel channels (Figs. 9 and 21a). It should be noted that all of the previously dated Neoproterozoic muscovites in the Middle Nappe and Sand Voe Group are located in the schistose coaxially-deformed domains that are sandwiched between shear zones with seemingly coeval antithetic and synthetic shear sense (i.e. top-to-the-NW thrusting and top-to-the-SE extension or top-to-the-NNE sinistral and top-to-the-SSW dextral) (Fig. 9). The extrusion of deformed rock units bounded by coeval, opposing faults or shear zones is a characteristic feature of most numerical deformation models that involve combinations of coaxial and non-coaxial strain (e.g. Sanderson and Marchini 1984; Jones et al., 1997, 2005). In the case of transpression, dip- and strike-parallel ductile extrusion have been modelled (e.g. Jones et al., 1997, 2005; Teyssier and Tikoff 1999; Fernández and Díaz-Azpiroz 2009) and documented in natural settings (Dias and Ribeiro 1994; Jones et al., 1997; Viola and Henderson 2010; Kuiper et al., 2011; Fernández et al., 2013; Massey and Moecher 2013; Sarkarinejad et al., 2013) to show unconfined shortening across the deformation belt. Using this model, antithetic deformation is a kinematic requirement, and it is not necessary to invoke a separate deformation event with opposing shear senses.

5.4. Metamorphic considerations

Mid-crustal ductile thrusting should place higher grade metamorphic rocks above lower grade, to result in metamorphic inversion (e.g. Rice et al., 1989; Hubbard 1996; Stephenson et al., 2000). This has been documented in detail in the Caledonides of northern mainland Scotland where there are marked increases in Scandian metamorphic grade from west to east with increasing structural level and across regionally significant ductile thrusts (e.g. Thigpen et al., 2013; Mako et al., 2019; Law et al., 2021). Notably, this simple pattern is not observed within the North Roe Nappe (Fig. 20). Instead, deformation temperatures (used here as a proxy for metamorphic grade) increase gradually upwards through the Lower and Middle nappes from c. 425 °C to c. 500 °C, but then appear to decrease to c. c. 400–375 °C above the Virdibreck Shear Zone (Fig. 20).

There are several potential explanations for this pattern and more than one may be applicable. One possibility is that the ductile thrusts cut through more steeply inclined metamorphic isograds to juxtapose higher level and lower grade rocks against deeper level and hotter rocks. However, this could also have been achieved if the Virdibreck Shear Zone was associated with early periods of top-to-the-NW extensional shear that cut down through gently-dipping to subhorizontal isograds prior to final reworking by sinistral strike-slip shearing. Further fabric and metamorphic studies may resolve this issue.

5.5. Older events and broader regional implications

The apparent pervasive nature of Scandian ductile deformation related to top-to-the-W/NW thrusting documented here west of the Walls Boundary Fault contrasts with the apparent dominance of older, Grampian structures to the east of the fault (Walker et al., 2020). Mainland Shetland, and Yell are dominated by a N-S trending, broadly upright foliation, associated with a gently plunging lineation. Kinematic indicators are largely absent, consistent with overall pure shear. Isotopic dating demonstrates that these structures formed between c. 470 and 465 Ma (Walker et al., 2016, 2020). They overprint an older gently dipping foliation and associated W-trending lineation, relics of which are preserved in NW Unst and are thought to have formed at an earlier stage (485–470 Ma) of the Grampian orogenic event during ophiolite obduction (Flinn and Oglethorpe 2005; Biejat et al., 2018). These differences in both structural style and timing of deformation either side of the WBF, likely reflect Scandian and younger strike-slip displacements along that structure (of uncertain magnitude) which juxtaposed different domains of the orogenic wedge, as well as presumed down-to-the-E displacement on the fault. Nonetheless, a basal Scandian detachment equivalent to the North Roe Thrust is assumed to underlie the entire area east of the WBF (Fig. 21b).

The only area east of the WBF where Scandian deformation has been documented is on Unst and Fetlar (Fig. 1b). Here, sinistrally oblique extensional, top-down-to-the-NNE, shear juxtaposed the lower ophiolite thrust sheets against their current footwall rocks (Cannat 1989; Biejat et al., 2018). The associated deformation fabrics are recorded in the Funzie Conglomerate on Fetlar and must be younger than its depositional age of <440 Ma (Biejat et al., 2018). Rb-Sr mica ages of 440–430 Ma obtained in west Unst are thought to date deformation (Walker et al., 2016). The generally northward-directed displacement here compares with that associated with the late sinistral fabrics in the North Roe Nappe. However, the final phase of Scandian deformation on Fetlar was associated with thrusting of the upper ophiolite nappe onto the already deformed Funzie Conglomerate. Hence the older phase of Scandian sinistrally oblique extension here might reflect gravitational instability within an overall regime of crustal thickening, rather than late orogenic transpression as manifested along the WBF (Watts et al., 2007; this study).

The deformation structures documented in NW Shetland compare closely with those described in related areas along the margin of the Laurentian Caledonides which similarly show evidence for strain partitioning during later stages of the Scandian orogenic event. In mainland northern Scotland, Scandian ductile thrusting was associated with a regional foreland-propagating, anticlockwise swing in transport directions from top-to-the-NNW to top-to-the-WNW (Kinny et al., 2019; Law and Johnson 2010; Krabbendam et al., 2021; Strachan et al., 2020; Law et al., 2021). Thrusting continued until at least c. 425 Ma and overlapped with the onset of sinistral strike-slip displacements along the Great Glen Fault (e.g. Stewart et al., 2001; Strachan et al., 2020). An almost identical foreland propagating rotation in thrust transport directions has been documented in NE Greenland. Here the later stages of Scandian thrusting there were inferred to have overlapped the onset of sinistral displacements along the orogen-parallel Storstrømmen shear zone (Holdsworth and Strachan 1991; Strachan et al., 1992; Smith et al., 2007), although in NE Greenland much of this deformation occurred during the Devonian (Dallmeyer et al., 1994; Hallett et al., 2014), reflecting the along strike diachroneity of collision. The evidence for Scandian transpression in NW Shetland thus complements published tectonic models that interpret the final stages of the Caledonian orogeny as being characterised by sinistrally oblique convergence between Laurentia and Baltica (e.g. Soper et al., 1992; Dewey and Strachan 2003).

6. Conclusions

The mainly greenschist to amphibolite-facies Precambrian rocks of the NRN preserve complex and heterogeneous combinations of coaxial and non-coaxial transpressional deformation. These formed during overprinting Neoarchaean, Neoproterozoic (Knoydartian) and Ordovician-Silurian (Caledonian) episodes. Detailed field and microstructural analyses show that the main ductile fabrics were formed during Caledonian (Scandian) top-to-the W/NW thrusting and top-to-the N sinistral shearing, with subordinate regions of top- to-the E extensional and NNE-SSW dextral shearing. In lower parts of the NRN, these different kinematic domains are texturally indistinguishable and overprinting relationships are absent. In contrast, top-to-the-west thrust-related fabrics are dominant in the upper NRN and are consistently overprinted by top-to-the-N/NE sinistral shearing. Further detailed geochronology is required to better refine the relative ages of metamorphism and deformation preserved in these complex ductilely deformed rocks. The area nevertheless illustrates vividly the kinematic complexity of natural transpression zones in mid-crustal settings.

CRediT authorship contribution statement

Timothy B. Armitage: Writing – original draft, Investigation, Data curation. **Robert E. Holdsworth:** Writing – review & editing, Supervision, Resources, Project administration, Methodology, Funding acquisition, Conceptualization. **Robin A. Strachan:** Writing – review & editing, Supervision, Conceptualization. **Edward D. Dempsey:** Writing – review & editing, Methodology, Formal analysis, Conceptualization. **Richard J. Walker:** Writing – review & editing, Visualization. **Diana T. Alvarez-Ruiz:** Methodology, Data curation. **Geoffrey E. Lloyd:** Writing – review & editing, Validation, Software, Data curation.

Declaration of competing interest

The authors declare that they have no known competing financial interests or personal relationships that could have appeared to influence the work reported in this paper.

Data availability

Data will be made available on request.

Acknowledgements

Rick Law is thanked warmly for discussions and advice at various stages in the development of this paper. Carlos Fernández, Dickson Cunningham and Anonymous are thanked for detailed reviews that led to significant strengthening of the EBSD analysis presented here, although the authors remain responsible for the final content of the paper. This work was supported by a NERC Doctoral Training Partnership grant NE/L002590/1 awarded to Armitage. This paper is published with permission of the Executive Director of the British Geological Survey (BGS-UKRI).

Appendix A. Supplementary data

Supplementary data to this article can be found online at https://doi.org/10.1016/j.jsg.2024.105088.

References

Allmendinger, R.W., Siron, C.R., Scott, C.P., 2017. Structural data collection with mobile devices: accuracy, redundancy, and best practices. J. Struct. Geol. 102, 98–112. https://doi.org/10.1016/j.jsg.2017.07.011.

Andrews, I., 1985. The deep structure of the Moine Thrust, southwest of Shetland. Scot. J. Geol. 21, 213–217. https://doi.org/10.1080/1023624021000019333.

Armitage, T.B., 2021. Structural and Geochronological Investigations into Mid-crustal Shear Zones, Shetland, Scottish Caledonides. Unpublished PhD thesis, University of Durham.

Armitage, T.B., Watts, L.M., Holdsworth, R.E., Strachan, R.A., 2021. Late Carboniferous dextral transpressional reactivation of the crustal-scale Walls Boundary Fault, Shetland: the role of pre-existing structures and lithological heterogeneities. J. Geol. Soc. 178, jgs2020–j2078. https://doi.org/10.1144/jgs2020-078.

Bachmann, F., Hielscher, R., Schaeben, H., 2010. Texture analysis with MTEX- Free and open source software toolbox. Solid State Phenom. 160, 63–68. https://doi.org/10.4028/www.scientific.net/SSP.160.63.

Biejat, S., Strachan, R.A., Storey, C.D., Lancaster, P.J., 2018. Evidence for an early silurian synorogenic basin within the metamorphic hinterland of the North Atlantic caledonides: insights from the U-Pb zircon geochronology of the Funzie conglomerate, Shetland, Scotland. Tectonics 37, 2798–2817. https://doi.org/10.1029/2018TC005050.

Bird, A.F., Thirlwall, M.F., Strachan, R.A., Manning, C.J., 2013. Lu-Hf and Sm-Nd dating of metamorphic garnet: evidence for multiple accretion events during the Caledonian orogeny in Scotland. J. Geol. Soc. 170, 301–317. https://doi.org/10.1144/jgs2012-083.

Cannat, M., 1989. Late caledonian northeastward ophiolite thrusting in the Shetland islands, U.K. Tectonophysics 169, 257–270. https://doi.org/10.1016/0040-1951(89)90090-5.

Chew, D.M., Strachan, R.A., 2014. The Laurentian Caledonides of Scotland and Ireland, vol. 390. Geological Society, London, Special Publications, pp. 45–91. https://doi.org/10.1144/SP390.16.

Cross, A.J., Prior, D.J., Stipp, M., Kidder, S., 2017. The recrystallized grain size piezometer for quartz: An EBSD-based calibration. Geophys. Res. Lett. 44, 6667–6674. https://doi.org/10.1002/2017GL073836.

Crowley, Q.G., Strachan, R.A., 2015. U-Pb zircon constraints on obduction initiation of the Unst Ophiolite: an oceanic core complex in the Scottish Caledonides? J. Geol. Soc. 172, 279–282. https://doi.org/10.1144/jgs2014-125.

Cutts, K.A., Hand, M., Kelsey, D.E., Wade, B., Strachan, R.A., Clark, C., Netting, A., 2009. Evidence for 930 Ma metamorphism in the Shetland islands, scottish caledonides: implications for neoproterozoic tectonics in the laurentia–baltica sector of rodinia. J. Geol. Soc. 166, 1033–1047. https://doi.org/10.1144/0016-76492009-006.

Cutts, K.A., Hand, M., Kelsey, D.E., Strachan, R.A., 2011. P-T constraints and timing of Barrovian metamorphism in the Shetland Islands, Scottish Caledonides: implications for the structural setting of the Unst ophiolite. J. Geol. Soc. 168, 1265–1284. https://doi.org/10.1144/0016-76492010-165.

Dallmeyer, R.D., Strachan, R.A., Henriksen, N., 1994. 40Ar/39Ar mineral age record in NE Greenland: implications for tectonic evolution of the North Atlantic Caledonides. J. Geol. Soc. London 151, 615–628. https://doi.org/10.1144/gsjgs.151.4.0615.

de Paola, N., Holdsworth, R.E., McCaffrey, K.J.W., 2005. The influence of lithology and pre- existing structures on reservoir-scale faulting patterns in transtensional rift zones. J. Geol. Soc. 162, 471–480. https://doi.org/10.1144/0016-764904-043.

Dewey, J.F., Strachan, R.A., 2003. Changing Silurian-Devonian relative plate motion in the Caledonides: sinistral transpression to sinistral transtension. J. Geol. Soc. 160, 219–229. https://doi.org/10.1144/0016-764902-085.

Dewey, J.F., Holdsworth, R.E., Strachan, R.A., 1998. Transpression and transtension zones. In: Holdsworth, R.E., Strachan, R.A., Dewey, J.F. (Eds.), Continental Transpressional and Transtensional Tectonics, 135. Spec. Publ. Geol. Soc. London, pp. 1–14. https://doi.org/10.1144/gsl.sp.1998.135.01.01.

Dewey, J.F., Dalziel, I.W.D., Reavy, R.J., Strachan, R.A., 2015. The Neoproterozoic to Mid- Devonian evolution of Scotland: a review and unresolved issues. Scot. J. Geol. 52 https://doi.org/10.1144/sjg2016-015, 112–112.

Dias, R., Ribeiro, A., 1994. Constriction in a transpressive regime: an example in the Iberian branch of the Ibero-Armorican arc. J. Struct. Geol. 16, 1543–1554. https://doi.org/10.1016/0191-8141(94)90032-9.

Faleiros, F.M., Moraes, R., Pavan, M., Campanha, G.A.C., 2016. A new empirical calibration of the quartz c-axis fabric opening-angle deformation thermometer. Tectonophysics 671, 173–182. https://doi.org/10.1016/j.tecto.2016.01.014.

Fernández, C., Díaz-Azpiroz, M., 2009. Triclinic transpression zones with inclined extrusion. J. Struct. Geol. 31, 1255–1269. https://doi.org/10.1016/j.jsg.2009.07.001.

Fernández, C., Czeck, D.M., Díaz-Azpiroz, M., 2013. Testing the model of oblique transpression with oblique extrusion in two natural cases steps and consequences. J. Struct. Geol. 54, 85–102. https://doi.org/10.1016/j.jsg.2013.07.001.

Flinn, D., 1962. On folding during three-dimensional progressive deformation. J. Geol. Soc. London 118, 385–433. https://doi.org/10.1144/gsjgs.118.1.03.

Flinn, D., 1965. On the symmetry principle and the deformation ellipsoid. Geol. Mag. 102, 36–45. https://doi.org/10.1017/S0016756800053851.

Flinn, D., 1977. Transcurrentfaults and associated cataclasis in Shetland. J. Geol. Soc. 133, 231–247. https://doi.org/10.1144/gsjgs.133.3.0231.

Flinn, D., 1985. The caledonides of Shetland. In: Gee, D.G., Sturt, B.A. (Eds.), The Caledonide Orogen—Scandinavia and Related Areas. Wiley, New York, pp. 1159–1171.

Flinn, D., 1988. The moine rocks of Shetland. Scot. J. Geol. 74–85.

Flinn, D., 1992. The history of the Walls Boundary Fault, Shetland: the northward continuation of the Great Glen Fault from Scotland. J. Geol. Soc. 149, 721–726. https://doi.org/10.1144/gsjgs.149.5.0721.

Flinn, D., 1993. New evidence that the high temperature hornblende-schists below the Shetland ophiolite include basic igneous rocks intruded during obduction of the 'cold' ophiolite. Scot. J. Geol. 29, 159–165.

Flinn, D., 2014. Geology of Unst and Fetlar in Shetland: Memoir for 1: 50 000 Geological Sheet 131 (Scotland) Unst and Fetlar, 131. British Geological Survey.

Flinn, D., Oglethorpe, R.J.D., 2005. A history of the Shetland ophiolite complex. Scot. J. Geol. 41, 141–148. https://doi.org/10.1144/sjg41020141.
Flinn, D., Frank, P.L., Brook, M., Pringle, I.R., 1979. Basement-cover relations in Shetland. Geological Society of London 8, 109–115.
Fossen, H., Tikoff, B., 1998. Extended Models of Transpression and Transtension, and Application to Tectonic Settings. Geological Society of London, pp. 15–33.
Hallett, B.W., McClelland, W.C., Gilotti, J.A., 2014. The timing of strike-slip deformation along the Storstrømmen Shear Zone, Greenland Caledonides: U-Pb zircon and titanite geochronology. Geosci. Can. 41, 19–45. https://doi.org/10.12789/geocanj.2014.14.038.
Harland, W.B., 1971. Tectonic transpression in caledonian spitsbergen. Geol. Mag. 108, 27–41. https://doi.org/10.1017/S0016756800050937.
Holdsworth, R.E., Strachan, R.A., 1991. Interlinked system of ductile strike slip and thrusting formed by Caledonian sinistral transpression in northeastern Greenland. Geology 19, 510–513.
Holdsworth, R.E., Morton, A., et al., 2019. The nature and significance of the faroe-Shetland terrane: linking archaean basement blocks across the North atlantic. Precambrian Res. 321, 154–171. https://doi.org/10.1016/j.precamres.2018.12.004.
Hubbard, M.S., 1996. Ductile shear as a cause of inverted metamorphism: example from the Nepal Himalaya. J. Geol. 104, 493–499. https://doi.org/10.1086/629842.
Jahn, I., Strachan, R.A., Fowler, M., Bruand, E., Kinny, P.D., Clark, C., Taylor, R.J.M., 2017. Evidence from U – Pb zircon geochronology for early neoproterozoic (Tonian) reworking of an Archaean inlier in northeastern Shetland , scottish caledonides. J. Geol. Soc. 174, 217–232. https://doi.org/10.1144/jgs2016-054.
Jakob, J., Andersen, T.B., Kjøll, H.J., 2019. A review and reinterpretation of the architecture of the south and south-central Scandinavian Caledonides—a magma-poor to magma-rich transition and the significance of the reactivation of rift inherited structures. Earth Sci. Rev. 192, 513–528. https://doi.org/10.1016/j.earscirev.2019.01.004.
Jakob, J., Andersen, T.B., Mohn, G., Kjøll, H.J., Beyssac, O., 2022. Revised tectono-stratigraphic scheme for the Scandinavian Caledonides and its implications for our understanding of the Scandian orogeny. In: Kuiper, Y.D., Murphy, J.B., Nance, R.D., Strachan, R.A., Thompson, M.D. (Eds.), New Developments in the Appalachian-Caledonian-Variscan Orogen, 554. Geological Society of America Special Paper, pp. 335–374. https://doi.org/10.1130/2022.2554(14.
Jiang, D., Lin, S., Williams, P.F., 2001. Deformation path in high-strain zones, with reference to slip partitioning in transpressional plate-boundary regions. J. Struct. Geol. 23, 991–1005. https://doi.org/10.1016/S0191-8141(00)00170-X.
Jones, R.R., Holdsworth, R.E., Bailey, W., 1997. Lateral extrusion in transpression zones: the importance of boundary conditions. J. Struct. Geol. 19, 1201–1217. https://doi.org/10.1016/S0191-8141(97)00034-5.
Jones, R.R., Holdsworth, R.E., Clegg, P., McCaffrey, K., Tavarnelli, E., 2004. Inclined transpression. J. Struct. Geol. 26, 1531–1548. https://doi.org/10.1016/j.jsg.2004.01.004.
Jones, R.R., Holdsworth, R.E., McCaffrey, K.J.W., Clegg, P., Tavarnelli, E., 2005. Scale dependence, strain compatibility and heterogeneity of three-dimensional deformation during mountain building: a discussion. J. Struct. Geol. 27, 1190–1204. https://doi.org/10.1016/j.jsg.2005.04.001.
Kinny, P.D., Strachan, R.A., et al., 2019. The Neoarchean Uyea gneiss complex, Shetland: an onshore fragment of the Rae craton on the European plate. J. Geol. Soc. 176, 847–862. https://doi.org/10.1144/jgs2019-017.
Krabbendam, M., Strachan, R., Prave, T., 2021. A new stratigraphic framework for the early Neoproterozoic successions of Scotland. J. Geol. Soc. https://doi.org/10.1144/jgs2021-054 jgs2021-054.
Kuiper, Y.D., Lin, S., Böhm, C.O., 2011. Himalayan-type escape tectonics along the superior boundary zone in Manitoba, Canada. Precambrian Res. 187, 248–262. https://doi.org/10.1016/j.precamres.2011.03.009.
Lancaster, P.J., Strachan, R.A., Bullen, D., Fowler, M., Jaramillo, M., Saldarriaga, A.M., 2017. U–Pb zircon geochronology and geodynamic significance of 'Newer Granite' plutons in Shetland, northernmost Scottish Caledonides. J. Geol. Soc. 174, 486–497. https://doi.org/10.1144/jgs2016-106.
Law, R.D., 2014. Deformation thermometry based on quartz c-axis fabrics and recrystallization microstructures: a review. J. Struct. Geol. 66, 129–161. https://doi.org/10.1016/j.jsg.2014.05.023.
Law, R.D., Johnson, M.R.W., 2010. Microstructures and crystal fabrics of the Moine Thrust zone and Moine Nappe: history of research and changing tectonic interpretations. Geol. Soc. Spec. Publ. 335, 443–503. https://doi.org/10.1144/SP335.21.
Law, R.D., Searle, M.P., Simpson, R.L., 2004. Strain, deformation temperatures and vorticity of flow at the top of the greater Himalayan slab, Everest Massif, Tibet. J. Geol. Soc. London 161, 305–320. https://doi.org/10.1144/0016-764903-047.
Law, R.D., Thigpen, J.R., Mazza, S.E., Mako, C.A., Krabbendam, M., Spencer, B.M., Ashley, K.T., Strachan, R.A., Davis, E.F., 2021. Tectonic transport directions, shear senses and deformation temperatures indicated by quartz c-axis fabrics and microstructures in a NW-SE transect across the moine and Sgurr Beag thrust sheets, Caledonian orogen of northern Scotland. Geosciences 11, 411.
Law, R.D., Strachan, R.A., Thirlwall, M.F. & Thigpen, J.R. (in pres). The Caledonian orogeny: Late Ordovician to Early Devonian tectonic and magmatic events associated with closure of the Iapetus Ocean. In: Smith, M. & Strachan, R.A. (editors) Geology of Scotland. fifth ed.. The Geological Society, London. https://doi.org/10.1144/GOS5-2022-71.
Lin, S., Jiang, D., Williams, P.F., Dewey, J.F., Holdsworth, R.E., Strachan, R.A., 1999. Discussion on transpression and transtension zones. J. Geol. Soc. London 156, 1045–1050.
Lloyd, G.E., 2020. Syntectonic quartz vein evolution during progressive deformation, 2020. In: BOND, C.E., LEBIT, H.D. (Eds.), Folding and Fracturing of Rocks: 50 Years of Research since the Seminal Text Book of J. G. Ramsay, vol. 487. Geological Society, London, Special Publications, pp. 127–151. https://doi.org/10.1144/SP487.3.
Lusk, A.D.J., Platt, J.P., Platt, J.A., 2021. Natural and experimental constraints on a flow law for dislocation-dominated creep in wet quartz. J. Geophys. Res. Solid Earth 126, e2020JB021302. https://doi.org/10.1029/2020JB021302.
Mako, C.A., Law, R.D., Caddick, M.J., Thigpen, J.R., Ashley, K.T., Cottle, J., Kylander-Clark, A., 2019. Thermal evolution orf the Scandian hinterland, Naver nappe, northern Scotland. J. Geol. Soc. London 176, 669–688, 10/1144/jgs.2018-244.
Massey, M.A., Moecher, D.P., 2013. Transpression , extrusion , partitioning , and lateral escape in the middle crust : Signi fi cance of structures , fabrics , and kinematics in the Bronson Hill zone , southern New England , U . S . A. J. Struct. Geol. 55, 62–78. https://doi.org/10.1016/j.jsg.2013.07.014.
McGeary, S., 1989. Reflection seismic evidence for a Moho offset beneath the Walls Boundary strike-slip fault. J. Geol. Soc. 146, 261–269. https://doi.org/10.1144/gsjgs.146.2.0261.
Mykura, W., Flinn, D., May, F., 1976. British Regional Geology: *Orkney and Shetland*. HMSO, Edinburgh.
Passchier, C.W., Trouw, R.A.J., 2005. Micro-Tectonics, second ed. Springer, New York, p. 366.
Prave, A.R., Strachan, R.A., Fallick, A.E., 2009. Global C cycle perturbations recorded in marbles: a record of Neoproterozoic Earth history within the Dalradian succession of the Shetland Islands, Scotland. J. Geol. Soc. 166, 129–135. https://doi.org/10.1144/0016-76492007-126.
Pringle, I.R., 1970. The structural geology of the North Roe area of Shetland. Geol. J. 7, 147–170. https://doi.org/10.1002/gj.3350070109.
Rice, A.H.N., Bevins, R.E., Robinson, D., Roberts, D., 1989. Thrust-related metamorphic inversion in the Caledonides of Finnmark, north Norway. In: Daly, J.S., Cliff, R.A., Yardley, B.W.D. (Eds.), Evolution of Metamorphic Belts, 43. Geological Society, London, Special Publication, pp. 413–421.
Ritchie, J.D., Hitchen, K., Mitchell, J.G., 1987. The offshore continuation of the Moine Thrust north of Shetland as deduced from basement isotopic ages. Scot. J. Geol. 23, 163–173. https://doi.org/10.1144/sjg23020163.
Roper, P.J., 1972. Structural significance of 'button' or 'fish scale' texture in phyllonitic schist of the brevard zone, northwestern South Carolina. Bull. Geol. Soc. Am. 83, 853–860. https://doi.org/10.1130/0016-7606(1972)83[853:SSOBOF]2.0.CO;2.
Sanderson, D.J., Marchini, W.R.D., 1984. Transpression. J. Struct. Geol. 6, 449–458. https://doi.org/10.1016/0191-8141(84)90058-0.
Sarkarinejad, K., Partabian, A., Faghih, A., 2013. Variations in the kinematics of deformation along the Zagros inclined transpression zone, Iran: Implications for defining a curved inclined transpression zone. J. Struct. Geol. 48, 126–136. https://doi.org/10.1016/j.jsg.2012.11.009.
Schmid, S.M., Casey, M., 1986. Complete fabric analysis of some commonly observed quartz c-axis patterns. In: Hobbs, B.E., Heard, H.C. (Eds.), Mineral and Rock Deformation: Laboratory Studies, Geophysics Monographs Series, 36. American Geophysical Union, Washington, DC, pp. 263–286. https://doi.org/10.1029/GM036p0263.
Smith, S.A.F., Strachan, R.A., Holdsworth, R.E., 2007. Microstructural evolution within a partitioned midcrustal transpression zone, northeast Greenland Caledonides. Tectonics 26, 1–20. https://doi.org/10.1029/2006TC001952.
Soper, N.J., Strachan, R.A., Holdsworth, R.E., Gayer, R.A., Greiling, R.O., 1992. Sinistral transpression and the Silurian closure of Iapetus. J. Geol. Soc. 149, 871–880. https://doi.org/10.1144/gsjgs.149.6.0871.
Spray, J.G., 1988. Thrust-related metamorphism beneath the Shetland Islands oceanic fragment, northeast Scotland. Can. J. Earth Sci. 25, 1760–1776.
Spray, J.G., Dunning, G.R., 1991. A U/Pb age for the Shetland Islands oceanic fragment, Scottish Caledonides: evidence from anatectic plagiogranites in ' layer 3' shear zones. Geol. Mag. 128, 667–671.
Stephenson, B., Waters, D., Searle, M.P., 2000. Inverted metamorphic and Main Central Thrust: field relations and thermobarometric constraints from the Kishtwar Window, NW Indian Himalaya. J. Metamorph. Geol. 18, 571–590. https://doi.org/10.1047/j.1525-1314.2000.0027.x.
Stewart, M., Strachan, R.A., Martin, M.W., Holdsworth, R.E., 2001. Constraints on early sinistral displacements along the Great Glen Fault Zone, Scotland: structural setting, U-Pb geochronology and emplacement of the syn-tectonic Clunes tonalite. J. Geol. Soc. 158, 821–830. https://doi.org/10.1144/jgs.158.5.821.
Stipp, M., Stünitz, H., Heilbronner, R., Schmid, S.M., 2002. The eastern Tonale fault zone: A 'natural laboratory' for crystal plastic deformation of quartz over a temperature range from 250 to 700 °C. J. Struct. Geol. 24, 1861–1884. https://doi.org/10.1016/S0191-8141(02)00035-4.
Strachan, R.A., Holdsworth, R.E., Friderichsen, J.D., Jepsen, H.F., 1992. Regional Caledonian structure within an oblique convergence zone, Dronning Louise Land, NE Greenland. J. Geol. Soc. 149, 359–371. https://doi.org/10.1144/gsjgs.149.3.0359.
Strachan, R.A., Prave, A.R., Kirkland, C.L., Storey, C.D., 2013. U–Pb detrital zircon geochronology of the Dalradian Supergroup, Shetland Islands, Scotland: implications for regional correlations and Neoproterozoic–Palaeozoic basin development. J. Geol. Soc. 170, 905–916. https://doi.org/10.1144/jgs2013-057.
Strachan, R.A., Alsop, G.I., Ramezani, J., Frazer, R.E., Burns, I.M., Holdsworth, R.E., 2020. Patterns of silurian deformation and magmatism during sinistral oblique convergence, northern scottish caledonides. J. Geol. Soc. 177, 893–910. https://doi.org/10.1144/jgs2020-039.
Stünitz, H., Fitz Gerald, J.D.F., 1993. Deformation of granitoids at low metamorphic grade. II: Granular flow in albite-rich mylonites. Tectonophysics 221, 299–324. https://doi.org/10.1016/0040-1951(93)90164-F.
Tavarnelli, E., Holdsworth, R.E., Clegg, P., Jones, R.R., McCaffrey, K.J.W., 2004. The anatomy and evolution of a transpressional imbricate zone, Southern Uplands,

Scotland. J. Struct. Geol. 26, 1341–1360. https://doi.org/10.1016/j.jsg.2004.01.003.
ten Grotenhuis, S.M., Trouw, R.A.J., Passchier, C.W., 2003. Evolution of mica fish in mylonitic rocks. Tectonophysics 372, 1–21. https://doi.org/10.1016/S0040-1951(03)00231-2.
Teyssier, C., Tikoff, B., 1998. Strike-slip Partitioned Transpression of the San Andreas Fault System: a Lithospheric-Scale Approach, 135. Geological Society Special Publication, pp. 143–158. https://doi.org/10.1144/GSL.SP.1998.135.01.10.
Teyssier, C., Tikoff, B., 1999. Fabric stability in oblique convergence and divergence. J. Struct. Geol. 21, 969–974. https://doi.org/10.1016/S0191-8141(99)00067-X.
Thigpen, J.R., Law, R.D., Loehn, C.L., Strachan, R.A., Tracey, R.J., Lloyd, G.E., Roth, B.L., Brown, S.J., 2013. Thermal structure and tectonic evolution of the Scandian orogenic wedge, Scottish Caledonides: integrating geothermometry, deformation temperatures, and conceptual kinematic-thermal models. J. Metamorph. Geol. 31, 813–842. https://doi.org/10.1111/jmg.12046.
Tullis, J., Yund, R.A., 1991. Diffusion creep in feldspar aggregates: experimental evidence. J. Struct. Geol. 13, 987–1000. https://doi.org/10.1016/0191-8141(91)90051-J.
Vernon, R.H., 2004. A Practical Guide to Rock Microstructure. Cambridge University Press, Cambridge. https://doi.org/10.1017/CBO9780511807206.
Viola, G., Henderson, I.H.C., 2010. Inclined transpression at the toe of an arcuate thrust: an example from the Precambrian "Mylonite Zone" of the Sveconorwegian orogen. In: Law, R.D., Butler, R.W.H., Holdsworth, R.E., Krabbendam, M., Strachan, R.A. (Eds.), Continental Tectonics and Mountain Building: the Legacy of Peach and Horne, vol. 335. Geological Society, London, Special Publications, pp. 707–727.
Walker, S., Thirlwall, M.F., Strachan, R.A., Bird, A.F., 2016. Evidence from Rb–Sr mineral ages for multiple orogenic events in the Caledonides of Shetland, Scotland. J. Geol. Soc. 173, 489–503. https://doi.org/10.1144/jgs2015-034.
Walker, S., Bird, A.F., Thirlwall, M.F., Strachan, R.A., 2020. Caledonian and Pre-caledonian Orogenic Events in Shetland, Scotland: Evidence from Garnet Lu-Hf and Sm-Nd Geochronology, vol. 503. Geological Society, London, Special Publications. https://doi.org/10.1144/sp503-2020-32. SP503-2020-2032.
Wallis, S.R., 1992. Vorticity analysis in a metachert from the Sanbagawa Belt, SW Japan. J. Struct. Geol. 14 (3), 271–280. https://doi.org/10.1016/0191-8141(92)90085-B.
Wallis, S.R., 1995. Vorticity analysis and recognition of ductile extension in the Sanbagawa belt, SW Japan. J. Struct. Geol. 17 (8), 1077–1093. https://doi.org/10.1016/0191-8141(95)00005-X.
Watts, L.M., Holdsworth, R.E., Sleight, J.A., Strachan, R.A., Smith, S.A.F., 2007. The movement history and fault rock evolution of a reactivated crustal-scale strike-slip fault: the Walls Boundary Fault Zone, Shetland. J. Geol. Soc. 164, 1037–1058. https://doi.org/10.1144/0016-76492006-156.
Woodcock, N.H., 1986. The role of strike-slip fault systems at plate boundaries. Phil. Trans. Roy. Soc. Lond. A317, 13–29.